Proximal C-terminus of α_{1C} subunits is necessary for junctional membrane-targeting of cardiac L-type calcium channels

Tsutomu Nakada[1], Bernhard E. Flucher[2], Toshihide Kashihara[1], Xiaona Sheng[1,3,4], Toshihide Shibazaki[1,5], Miwa Horiuchi-Hirose[1], Simmon Gomi[1,6], Masamichi Hirose[7], and MitsuhikoYamada[1,*].

[1]Department of Molecular Pharmacology, Shinshu University School of Medicine, Matsumoto, Nagano, Japan, [2]Department of Physiology and Medical Physics, Innsbruck Medical University, Innsbruck, Austria, [3]Department of Metabolic Regulation, Institute on Aging and Adaptation, Shinshu University Graduate School of Medicine, Matsumoto, Nagano, Japan. [4]Department of Neurology, The second Hospital of Hebei Medical University, Shijiazhuang, China [5]Discovery Research Laboratory II, R&D, Kissei Pharmaceutical Co., Ltd, Azumino, Nagano, Japan, [6]Department of Cardiovascular Medicine, Shinshu University School of Medicine, Matsumoto, Nagano, Japan, and [7]Department of Molecular and Cellular Pharmacology, School of Pharmaceutical Sciences, Iwate Medical University, Morioka, Iwate, Japan.

Short title: Junctional membrane-targeting motif of α_{1C}

Key words: Excitation-contraction coupling, Junctional membrane complex, $Ca_V1.2$, Cardiac myocyte, Couplon.

Abbreviations used: LTCC, L-type calcium channel; RyR, ryanodine receptor; JM, junctional membrane; EC, excitation-contraction; SR, sarcoplasmic reticulum; VDCR, voltage-dependent Ca^{2+} release; CICR, Ca^{2+}-induced Ca^{2+}release; CaM, calmodulin; DM, differentiation medium; DMEM, Dulbecco's Modified Eagle Medium; DCT, distal C-terminus; PCRD, proximal C-terminal regulatory domain; DCRD, distal C-terminal regulatory domain.

*Address to correspondence:
Mitsuhiko Yamada, MD, Ph.D.
3-1-1 Asahi, Matsumoto, Nagano 390-8621 Japan.
FAX: +81-263-37-3085
TEL: +81-263-37-2605
E-mail: myamada@shinshu-u.ac.jp

SYNOPSIS

In cardiac myocytes, L-type calcium channels (LTCC) form a functional signaling complex with ryanodine receptors at the junctional membrane (JM). Although the specific localization of LTCCs to JM is critical for excitation-contraction coupling, their targeting mechanism is unclear. Transient transfection of GFP-α_{1S} or GFP-α_{1C} but not P/Q type calcium channel α_{1A} in dysgenic (α_{1S}-null) GLT myotubes results in correct targeting of these LTCCs to the JMs and restoration of action potential-induced Ca^{2+} transient. To identify the sequences of α_{1C} responsible for the JM-targeting, we generated a range of α_{1C}/α_{1A} chimeras, deletion mutants and alanine substitution mutants and studied their targeting properties in GLT myotubes. The results revealed that amino acids ^{1681}LQAGLRTL^{1688} and ^{1693}PEIRRAIS^{1700} predicted to form two adjacent α-helices in the proximal C-terminus are necessary for the JM-targeting of α_{1C}. Efficiency of restoration of action potential-induced Ca^{2+} transient in GLT myotubes was significantly decreased by mutations in the targeting motif. The JM-targeting was not disrupted by the distal C-terminus of α_{1C} that binds to the second α-helix. Therefore, we identified a new structural motif in the C-terminus of α_{1C} that mediates the targeting of cardiac LTCC to JMs independently of the interaction between proximal and distal C-termini of α_{1C}.

INTRODUCTION

Voltage-dependent L-type calcium channels (LTCCs) play important roles in regulation of a variety of cellular functions of excitable cells, including excitation-contraction (EC) coupling, hormone secretion and transcriptional regulation [1, 2]. LTCCs are composed of the pore-forming α_{1S} ($Ca_V1.1$), ancillary β_1, $\alpha_2\delta$, and γ subunits in skeletal muscle cells, and of α_{1C} ($Ca_V1.2$), β_2, and $\alpha_2\delta$ subunits in cardiac muscle [3]. An α_1 subunit comprises four homologous repeats (I-IV), each containing six transmembrane segments (S1-S6) that together form the Ca^{2+} channel pore, the voltage sensor and activation and inactivation gates [4].

LTCCs in skeletal and cardiac muscle cells are specifically localized to the junctional membrane (JM) of the triad or peripheral couplings, where sarcolemmal membranes are closely apposed to the membranes of the terminal cisternae of the sarcoplasmic reticulum (SR) [5-7]. Ryanodine receptors (RyRs) are concentrated in the terminal cisternae and form a functional complex with LTCCs. In skeletal muscle cells, the pore-forming α_{1S} subunit directly interacts with the RyR1 through its cytoplasmic II-III loop and induces voltage-dependent Ca^{2+} release (VDCR) from SR in response to membrane depolarization. On the other hand, cardiac LTCCs induce EC coupling by Ca^{2+}-induced Ca^{2+}release (CICR). Whether cardiac EC coupling requires physical interaction of LTCCs with RyRs is a matter of debate. However, a rapid increase in the local Ca^{2+} concentration by LTCC openings in the vicinity of RyRs is essential for efficient CICR in cardiac myocytes [8, 9]. Thus, despite the difference in the Ca^{2+} release mechanisms, the precise colocalization of LTCCs with RyRs in JM is essential for normal EC coupling in both skeletal and cardiac muscle cells.

Although identification of the JM-targeting mechanisms of α_{1C} is critical for understanding how functional LTCC/RyR signaling complexes are formed and normal EC coupling is maintained in cardiac myocytes, the JM-targeting motif of α_{1C} is still unknown. This is in part due to the fact that isolated cardiac myocytes in primary culture are not suitable for these analyses because of their poor viability, rapid change in a cell shape and phenotype and their resistance to liposome-based transfection. Therefore, in the past the plasma membrane targeting signal of α_{1C} was analyzed in non-muscle cells, such as tsA201 cells, leading to the identification of a role of the C-terminus [10]. Furthermore, LTCCs were coexpressed with RyRs in Chinese hamster ovary cells in previous studies [11, 12]. However, these cells did not exhibit the Ca^{2+} release from endoplasmic reticulum in response to membrane depolarization [11, 12], indicating that the functional calcium releasing complex of LTCCs and RyRs could not be reconstituted. Thus, these cells are not suitable for the analysis of the JM-targeting motif of α_{1C}. To overcome these problems, we utilized GLT cells, a muscle cell line derived from α_{1S}-deficient dysgenic (*mdg*) mice [13]. In dysgenic myotubes transiently expressed α_{1S} (with N-terminal GFP-tag) is correctly localized to JM with RyRs and restores skeletal LTCC currents, VDCR and EC coupling [14-16]. Moreover this muscle expression system has previously been used to identify a 55 amino acid sequence in the C-terminus of $Ca_V1.1$ that is important for JM targeting of the skeletal muscle calcium channel. Importantly, heterologously expressed cardiac α_{1C} is also colocalized with RyRs in the JM of GLT myotubes and restores cardiac type CICR and EC coupling [14, 17]. Thus, GLT cells express the machinery required for the JM-targeting of α_{1C} and therefore are a suitable cell system to analyze the mechanism underlying the JM-targeting of the cardiac LTCC α_{1C} subunit.

In this study, we constructed multiple α_{1C}-based α_{1C}/α_{1A} chimeras and mutants, expressed them in GLT cells and analyzed their subcellular localizations with immunofluorescence staining. The results identify a novel targeting motif consisting of two adjacent α-helices within amino acid residues 1681–1700 at the proximal C-terminus of α_{1C} that are necessary for the JM-targeting. The distal half of the JM-targeting motif overlaps with sequences to which the proteolytically cleaved distal C-terminus binds [18-20]. This interaction is essential for β-adrenergic stimulation of LTCCs [21]. However, the JM-targeting of α_{1C} was not compromised by expression of the distal C-terminus. Therefore, a new structural motif in the C-terminus of α_{1C} identified in this study mediates the

specific targeting of the cardiac LTCC to JMs of the EC coupling apparatus without interfering with the interaction between the proximal and distal C-termini of α_{1C}.

EXPERIMENTAL

Plasmid construction

The cDNA encoding rabbit α_{1C} was generously given by Prof. William Catterall (University of Washington). The cDNAs encoding GFP-α_{1A} and -α_{1M} were generously supplied by Prof. Manfred Grabner (Innsbruck Medical University). Most chimera constructs were prepared with a "gene SOEing" technique [22]. All primer sequences used in this study are available upon request. DNA polymerase PrimeSTAR HS (Takara Bio, Shiga, Japan) was used for all PCR reactions. To generate GFP-α_{1C}, the cDNA of rabbit α_{1C} was amplified by PCR and then subcloned into *Hin*dIII/*Sal*I sites of pEGFP-C1. An HA-epitope was inserted into the extracellular loop between S5 and S6 in domain II of α_{1C} as previously described (HA-α_{1C}) [23, 24]. Chimera constructs (GFP-$\alpha_{1C}NT_A$, GFP-α_{1C}I-II_A, GFP-α_{1C}II-III_M, GFP-□α_{1C}III-IV_A, GFP-$\alpha_{1C}CT_A$, HA-$\alpha_{1C}1507–1650_A$, HA-$\alpha_{1C}1624–1665_A$, HA-$\alpha_{1C}1666–1733_A$, HA-$\alpha_{1C}1666–1676_A$, HA-$\alpha_{1C}1666–1688_A$, HA-$\alpha_{1C}1677–1688_A$, HA-$\alpha_{1C}1689–1733_A$, HA-$\alpha_{1C}1709–1733_A$, GFP-$\alpha_{1A}CT_C$, GFP-$\alpha_{1A}JMT_C$, and CD8-α_{1C}CT) were prepared by a SOEing technique. Two or three fragments of PCR products were fused and subcloned into a blunt-ended pZErO-2 vector (Invitrogen, Carlsbad, CA) and then back to corresponding region of each vectors (GFP□α_{1C}, GFP-α_{1A}, or HA-α_{1C}) using additional or native restriction sites. The deletion mutants (HA-$\alpha_{1C}\Delta1821$, HA-$\alpha_{1C}\Delta1733$, HA-$\alpha_{1C}\Delta1666$, and HA-$\alpha_{1C}\Delta1624$) were generated by PCR using antisense primers containing a stop codon and *Sal*I restriction site. The PCR products were subcloned into a blunt-ended pZErO-2 vector and again subcloned into the *Eco*RV/*Sal*I site of HA-α_{1C}. Alanine substitution mutants were generated with the QuickChange Site-Directed Mutagenesis Kit (Stratagene) according to manufacturer's instruction.

The distal C-terminus of α_{1C} (1821–2171) was amplified by PCR and then subcloned into p3×FLAG-CMV10. The cDNAs of calmodulin (CaM), sorcin, and CD8a were isolated with RT-PCR from mouse heart and blood cDNA. The cDNAs of CaM and sorcin were subcloned into p3×FLAG-CMV10. The calcium-insensitive mutant CaM_{1234} (D21A/D57A/D94A/D130A) was prepared with the QuickChange Site-Directed Mutagenesis Kit according to manufacture's instruction. CD8a and CD8a-α_{1C}CT were subcloned into pcDNA3.1. The nucleotide sequences of all the constructs were verified with ABI 3130 (Applied Biosystems, Foster City, CA).

Cell culture and transfection

Myotubes of the GLT cell line derived from myoblasts of dysgenic (*mdg*) mice were cultured as previously described [13]. Briefly, GLT cells were plated on carbon coated coverslips coated with 0.1% gelatin (day 0) in growth medium (GM): Low Glucose Dulbecco's Modified Eagle Medium (DMEM, Invitrogen) containing GlutaMAX (Invitrogen), 10% fetal bovine serum (FBS), 10% horse serum, 100-U penicillin and 100-µg streptomycin. To differentiate myoblasts to the myotubes, two days after plating (day 2), the medium was changed to differentiation medium (DM): DMEM containing 2% horse serum (Invitrogen), GlutaMAX (Invitrogen), 100 U penicillin and 100 µg streptomycin (Invitrogen). Again two days later (day 4), cells were transfected with the expression vectors using FuGene HD (Roche Diagnostics, Basel, Switzerland) according to manufacturer's instruction (1 µg plasmid DNA/35-mm dish). For coexpression of channels and other proteins (CaM_{WT}, CaM_{1234}, and sorcin), equal amounts of both plasmid DNA (0.75 µg) were transfected. Plasmid vectors coding for channels ($\alpha_{1C}\Delta1821$ or α_{1C}) and the distal C-terminus (DCT) of α_{1C} were co-transfected with various molar ratio in the GLT myotube (DCT/channel vectors molar ratios were 0.8, 1.6, and 3.2). Between day 7-10 myotubes were fixed and immunofluorescence labeling was performed.

Immunofluorescence staining

Cells were fixed in 4% paraformaldehyde in phosphate buffered saline (PBS) at room temperature for 10 min. After washing the samples with PBS, cells were blocked and permeabilized with PBS containing 0.2% Triton and 5% FBS for 1 hour at room temperature and then incubated with primary

antibodies at 4ºC for overnight. After washing with PBS, cells were incubated with fluorescent dye-conjugated secondary antibodies and Hoechst 33342 (Dojindo, Kumamoto, Japan) at room temperature for 1h. Cells were again washed with PBS, and coverslips were mounted with Fluoromount-G (Beckman Coulter, Fullerton, CA). To label extracellular HA-epitope or CD8, cells were incubated with the corresponding primary antibodies at 37ºC for 60 min before permeabilization. The following primary and secondary antibodies were used: anti-GFP rabbit polyclonal antibody (Invitrogen, 1:1000 dilution), anti-ryanodine receptor mouse monoclonal antibody (Affinity bioreagents, Golden, CO, clone 34C, 1:1000), anti-HA rat monoclonal antibody (Roche Diagnostics, clone 3F10, 1:200), anti-mouse CD8a rat monoclonal antibody (BioLegend, San Diego, CA, clone 53-6.7, 1:1000), anti-FLAG M2 mouse monoclonal antibody (Sigma, 1:1000), Alexa Fluor 488 goat anti-rabbit IgG (Invitrogen), anti-myosin heavy chain mouse monoclonal antibody (R&D systems, Minneapolis, MN, clone MF20, 1:100), Alexa Fluor 488 goat anti-mouse IgG (Invitrogen) and Alexa Fluor 555 goat anti-rat antibody (Invitrogen). Fluorescence images were acquired with an LSM 5 exciter laser scanning microscope (Carl Zeiss, Thornwood, NY). At least 200 transfected-myotubes were analyzed for each clone, and representative photos are shown in figures. To quantify the efficiency of targeting of each construct to JM, the percentage of myotubes showing LTCC clustering relative to the total number of LTCC expressing myotubes was assessed. For each construct, 3-5 coverslips (40-205 myotubes/coverslip) were tested to obtain means ± S.E.M. A myotube was classified as "clustered" if any region of the myotube displayed the characteristic clustered immunolabeling pattern.

To verify that under non-permeabilized conditions the anti-HA-antibody recognized only membrane-targeted proteins, permeabilized and non-permeabilized myotubes were stained in parallel (Fig. S1). The fluorescence signal in the ER/SR under the permeabilized condition was very intensive compared with that in the plasma membrane under the non-permeabilized condition. No non-permeabilized myotubes exhibited such intense ER/SR signal, indicating that under non-permeabilized conditions the anti-HA-antibody detected exclusively membrane-targeted proteins. Under the permeabilized condition, a clustered distribution was observed in ~20% of myotubes transfected with HA-α_{1C} and in 57% of myotubes transfected with GFP-α_{1C} (Table 1). Apparently differently high expression levels of the two constructs in the ER/SR system mask the label of membrane-expressed channels to different degrees.

Using a colocalization function of ZEN program (Carl Zeiss), colocalization coefficient of HA-tagged channels with RyR signals was calculated as $P_{HA+RyR}/P_{HAtotal}$, where P_{HA+RyR} and $P_{HAtotal}$ are the number of pixels containing both HA and RyR signals and those containing HA signals, respectively. All of the images were acquired with the same microscope and camera setting, and individual myotubes were selected by ROI (region of interest) tool for calculation.

Ca^{2+} imaging

GLT myotubes cultured on carbon-coated coverslips (113 mm^2) were incubated with 5 μM Fluo-4-AM (Dojindo) plus 0.01% Cremophore EL (Sigma) and 0.02% bovine serum albumin (Sigma) in serum-free DMEM for 45 min at 37ºC followed by de-esterification. Myotubes were superfused with the modified Tyrode solution (136.5 mM NaCl, 5.4 mM KCl, 1.8 mM $CaCl_2$, 0.53 mM $MgCl_2$, 5.5 mM HEPES, and 5.5 mM glucose, pH 7.4) at room temperature and paced with 1-ms pulses of 50 V at 0.3 Hz across the 20-mm incubation chamber. Fluorescence images were acquired with an LSM 7 LIVE laser scanning microscope with a 20x/0.8 plan apochromatic objective (Carl Zeiss). Fluo-4 was excited by 488 nm light, and emission light passed through a high-pass filter of 495 nm and imaged with a CCD camera. Each image was taken with 128 x 128 pixels every 2.8 msec. The time course of Ca^{2+} transients was obtained from fluorescence change in individual myotubes selected by ROI tool. To block Ca^{2+} influx through plasma membrane, 0.5 mM Cd^{2+} and 0.1 mM La^{3+} were added. Application of 6 mM caffeine proved the functionality of SR Ca^{2+} release.

For quantification of the numbers of channel-expressing myotubes, cultures on coverslip were stained with anti-HA or anti-GFP, and anti-myosin heavy chain (differentiation marker) antibodies in

permeabilized condition (see Immunofluorescence staining section). Low magnification (10x objective) fluorescence images were acquired 5 randomly selected areas of each specimen, and quantified the number of myotube expressed all of HA or GFP and myosin heavy chain.

Statistical analysis

Data are shown as the means ± S.E.M. Statistical significance was evaluated with Student's unpaired *t*-test. For the multiple comparisons of data, analysis of variance with Bonferroni's test was used. $p < 0.05$ was considered significant.

RESULTS

The C-terminal domain is necessary for JM-targeting of the α_{1C} subunit.

Previous studies revealed that transiently transfected α_{1S} subunits of skeletal muscle LTCCs but not α_{1A} subunits of neuronal P/Q type calcium channels were localized to JM in GLT myotubes [14, 15]. These studies further showed that heterologously expressed α_{1C} subunits of cardiac LTCCs were also targeted to JM and supported CICR in GLT myotubes [17, 25]. Thus, by using the same muscle expression system, we now sought to identify the critical motif of α_{1C} subunits for JM-targeting. We made several chimeras and transiently expressed them in GLT cells (Fig. 1A). The N-terminus ($\alpha_{1C}NT_A$), I-II loop (α_{1C}I-II$_A$), III-IV loop (α_{1C}III-IV$_A$) and C-terminus ($\alpha_{1C}CT_A$) of α_{1C} were substituted with corresponding regions of α_{1A}. Since the II-III loop of α_{1A} is >3 times longer than that of α_{1C}, a chimera with the II-III loop of house fly (*M. domestica*) α_1 (α_{1C}II-III$_M$) [14, 26] was used instead to examine the role of the II-III loop chimera in JM targeting. House fly α_1 subunits were not targeted to JM in GLT myotubes (data not shown). All chimeras were fused with GFP at the N-terminus of α_{1C}.

The localization of the GFP-α_{1C} and related chimeras relative to JM identified by anti-RyR was assessed by immunofluorescence labeling. GFP-α_{1C} showed a clustered distribution and was colocalized with RyRs in JM as previously reported (Fig. 1B). The quantitative results of the clustering assay of all channels tested in this study are shown in Table 1. GFP-$\alpha_{1C}NT_A$, GFP-α_{1C}I-II$_A$, GFP-α_{1C}II-III$_M$, and GFP-α_{1C}III-IV$_A$ exhibited a localization virtually identical to that of GFP-α_{1C}, whereas GFP-$\alpha_{1C}CT_A$ was not clustered or colocalized with RyRs (Fig. 1C). The distribution of GFP-$\alpha_{1C}CT_A$ was very similar to that of α_{1A}, which was mainly localized in the ER/SR system and did not form clusters with RyRs (Fig. 1B) [13, 14]. These results indicated that the C-terminus of α_{1C} is necessary for the JM-targeting of α_{1C}. Although the JM-targeting rate of GFP-α_{1C}III-IV$_A$ was reduced to ~24% of that of GFP-α_{1C}, a considerable number of cells still exhibited a clustered distribution of the chimera (Table 1), indicating that the III-IV loop is not indispensable for the JM-targeting of α_{1C}.

The proximal C-terminus is necessary for JM-targeting of α_{1C}.

To determine the sequences within the C-terminus critical for JM targeting, we next tested C-terminal truncation mutants of α_{1C} and α_{1C}/α_{1A} chimeras. It is noteworthy that the C-terminus of α_{1C} is also important for plasma membrane expression of α_{1C} [10]. To assess JM-targeting of chimera proteins that were properly trafficked to the plasma membrane, we used an α_{1C} construct with an HA-epitope inserted into the extracellular loop between S5 and S6 segments in the domain II of α_{1C} (HA- α_{1C})[23, 24] for the construction of these mutants. Membrane-expressed channels were detected by anti-HA antibody labeling without prior membrane permeabilization. Successful expression of all of HA-tagged channels was confirmed with Western blotting (Fig. S2).

We analyzed JM-targeting with the following deletion mutants (Fig. 2A): An HA-$\alpha_{1C}\Delta$1821 mutant lacking the distal part of C-terminus, which is known to be subject to proteolytic cleavage in cardiac myocytes [20]; an HA-$\alpha_{1C}\Delta$1733 mutant further lacking the region corresponding to the JM-targeting motif of α_{1S} [14]; an HA-$\alpha_{1C}\Delta$1666 mutant lacking the whole C-terminus distal to the IQ motif; and an HA-$\alpha_{1C}\Delta$1624 mutant lacking the membrane-targeting motif identified previously [10]. Immunofluorescence analysis of transfected myotubes revealed the clustered distributions of HA-α_{1C}, HA-$\alpha_{1C}\Delta$1821 and HA-$\alpha_{1C}\Delta$1733 (>75% of cells, $n \geq 200$) (Figs. 2B and 2C and Table 1). In contrast, HA-$\alpha_{1C}\Delta$1666 was diffusely distributed in the plasma membrane (Fig. 2B), suggesting that amino acids between 1666 and 1733, but not those distal to1733 are necessary for the JM-targeting of α_{1C}. Colocalization coefficient of HA-$\alpha_{1C}\Delta$1666 with RyR was significantly decreased compared to HA-α_{1C} (Fig. 2D). No fluorescence signal was observed in myotubes transfected with HA-$\alpha_{1C}\Delta$1624 (Fig. S1).

Next we analyzed three α_{1C}-based chimeras in which partially overlapping sequences of the

proximal C-terminus containing the critical domain between 1666 and 1733 were replaced with the corresponding sequences of α_{1A} (Fig. 2A). Substitution of 1507–1650 or 1624–1665 did not affect channel clustering, but chimera 1666–1733 failed to cluster in JM (Figs. 2C and D). Thus, amino acid residues 1666–1733 but not 1507–1665 or 1734–2171 in the C-terminus of α_{1C} are necessary for the proper JM-targeting.

To further narrow down the JM-targeting motif, we prepared four partially overlapping α_{1C}/α_{1A} chimeras within this critical region of the C-terminus (substitutions of 1666–1676, 1666–1688, 1689–1733 and 1709–1733) (Fig. 2A). Of these the two chimeras with substitutions of the peripherally located sequences HA-α_{1C}1666–1676$_A$ and HA-α_{1C}1709–1733$_A$ were correctly clustered in myotubes (Figs. 2C and D). In contrast both chimeras with substitutions of the central sequences HA-α_{1C}1666–1688$_A$ or HA-α_{1C}1689–1733$_A$ failed to cluster in JMs. These results limit the sequences in the C-terminus of α_{1C} necessary for JM targeting to the 31 amino acid residues between 1677 and 1708.

To determine critical domains within this sequence we performed systematic alanine-scanning between 1677 and 1708. Within this sequence four consecutive amino acid residues at a time were sequentially substituted with alanines (Fig. 3). The numbers of the cells with α_{1C} clusters was dramatically decreased with the AAAA mutation of 1681–1684 (12%) and 1685–1688 (7%). A small but still significant decrease of clustering rates was also observed with AAAA mutations in 1689–1692 (78%), 1693–1696 (60%) and 1697–1700 (24%). In contrast, the clustering rates of AAAA mutants 1677–1680, 1701–1705, and 1705–1708 were not significantly different from those of wild type α_{1C} (Fig. 3B). Significant decrease of colocalization coefficient was observed with the AAAA mutations in 1681–1684, 1685–1688, and 1697–1700, but not 1689–1692 and 1693–1696 (Fig. 3C). Together these analyses demonstrate that the 20 amino acid residues 1681-1700 are necessary for the proper JM-targeting of α_{1C} and that within this sequence two motifs (^{1681}LQAGLRTL^{1688} and ^{1693}PEIRRAIS^{1700}) are of particular importance for the targeting mechanism.

The C-terminus of α_{1C} is not sufficient to confer JM-targeting property of α_{1C} to α_{1A} or CD8.
To assess whether the C-terminal targeting motif of α_{1C} can confer JM-targeting property to neuronal calcium channels or unrelated transmembrane proteins, we generated following three chimeras: the intracellular C-terminal domain of CD8 was replaced with the entire C-terminus of α_{1C} (CD8-α_{1C}CT); the JM-targeting motif of α_{1C} was substituted for the corresponding sequences of GFP-α_{1A} (GFP-α_{1A}JMT$_C$); and the entire C-terminus of GFP-α_{1A} was swapped with that of α_{1C} (GFP-α_{1A}CT$_C$). However, none of these three chimeras was clustered in JM (n > 200) (Fig. 4). These results indicate that, although the C-terminus of α_{1C} is necessary for the JM-targeting it is not sufficient.

The effect of transient expression of proteins interacting with the motif necessary for JM-targeting of α_{1C}.
In cardiac myocytes the distal C-terminus of α_{1C} (DCT) is truncated by proteolytic processing and the cleaved DCT re-associates with the proximal C-terminal regulatory domain (PCRD) (amino acid residues 1694–1700) of the truncated channel [18-20]. The interaction of DCT and PCRD auto-inhibits LTCCs and protein kinase A augments LTCC currents by removing this inhibition. This is a vital regulation of LTCCs in the flight-or-fight response [21]. Interestingly the distal half of the motif necessary for the JM-targeting of α_{1C} overlaps with PCRD. Thus, we assessed the effects of coexpression of DCT (α_{1C}1821–2171) on JM-targeting of HA-$\alpha_{1C}\Delta$1821 and HA-α_{1C} to examine if DCT inhibits the JM-targeting. However, coexpressed DCT did not reduce the JM-targeting of either one of these proteins (Fig. 5), indicating that the JM-targeting of α_{1C} would not disrupt the responsiveness of LTCCs to PKA.
The motif (1681–1700) necessary for JM-targeting of α_{1C} is immediately distal to the IQ-motif known to be the Ca^{2+}/CaM interaction site [27, 28]. Also the Ca^{2+}-binding protein sorcin is known to bind to amino acid residues 1622–1748 in the C-terminus of α_{1C} [29]. Thus, we examined the possibility

whether coexpression of CaM, its calcium-insensitive mutant (CaM_{1234}), or sorcin interferes with the JM-targeting of α_{1C}. However, coexpression of none of these proteins significantly altered the clustering rates of the HA-α_{1C} (Fig. S3).

Effect of mutations within the JM-targeting motif on EC coupling of α_{1C}.
Previous studies showed that transient expression of α_{1C} but not α_{1A} restored cardiac-type CICR in GLT myotubes [14, 25]. Thus, we examined whether JM-targeting contributed to the restoration of CICR by measuring action potential-induced Ca^{2+} transients of myotubes transfected with HA-α_{1C}, HA-α_{1C}1685AAAA1688, or HA-$\alpha_{1C}1666–1733_A$. Transient expression of HA-α_{1C} restored action potential-elicited Ca^{2+} transients (Fig. 6A). Complete block of the Ca^{2+} transients by dantrolene (100 μM), an inhibitor of RyR, (data not shown) identifies the SR as the major Ca^{2+} source. Cd^{2+}/La^{3+} abolished the Ca^{2+} transients whereas caffeine subsequently applied induced a large Ca^{2+} transient, indicating that the action potential-induced SR Ca^{2+} release required LTCC currents. Thus, HA-α_{1C} restored CICR. Interestingly, transfection with two constructs which failed to show JM-targeting, HA-α_{1C}1685AAAA1688 and HA-$\alpha_{1C}1666–1733_A$, also restored Ca^{2+} transients (Fig. 6A), indicating that these mutations did not disturb channel activity. Figure 6B shows that these constructs, however, were significantly less efficient than HA-α_{1C} in restoring the Ca^{2+} transients. Nevertheless, there was no significant difference between the mutant constructs and WT in the time-to-peak (HA-α_{1C}: 0.389 ± 0.037 s, HA-α_{1C}1685AAAA1688: 0.389 ± 0.036 s, HA-$\alpha_{1C}1666–1733_A$: 0.327 ± 0.035 s) or the peak amplitudes (HA-α_{1C}: 0.381 ± 0.028, HA-α_{1C}1685AAAA1688: 0.429 ± 0.055, HA-$\alpha_{1C}1666–1733_A$: 0.445 ± 0.061) of the restored Ca^{2+} transients. We also tested GFP-α_{1A}- or GFP-$\alpha_{1A}CT_C$-transfected myotubes. However, with these constructs no myotubes showed action potential-elicited Ca^{2+} transients (Fig. 6B). The number of channel-expressing myotubes in each dish was not significantly different among the groups (Figs. 6C and S4).

DISCUSSION

In this study, we identified amino acids residues 1681–1700 in the proximal C-terminus of α_{1C} as the motif necessary for the JM-targeting of α_{1C}. Systematic alanine-scanning in this sequence further showed that two separate motifs (^{1681}LQAGLRTL^{1688} and ^{1693}PEIRRAIS^{1700}) are of particular importance for the targeting mechanism. Using HEK tsA201 cells, Gao et al. showed that deletion of amino acid residues 1623–1666 of C-terminus completely disrupted the plasma membrane localization and clustering of α_{1C} and thus suggested that the sequence is a membrane-targeting motif [10]. This is consistent with our finding that HA-$\alpha_{1C}\Delta$1666 but not HA-$\alpha_{1C}\Delta$1624 was expressed in the plasma membrane in GLT myotubes (Fig. 2 and Fig. S1). However Gao et al., showed that the deletion of amino acids 1668–1733 of α_{1C} harboring the JM-targeting motif resulted in an only slightly decreased membrane targeting rate (90% in WT and 72% in $\alpha_{1C}\Delta$1668–1733) and did not disrupt the clustering of α_{1C} [10]. Thus, HEK tsA201 cells share with GLT cells the common mechanism for membrane targeting of α_{1C}, but their clustering mechanism does not resemble JM-targeting in muscle cells. In contrast, GLT myotubes support JM-targeting of α_{1S} as well as α_{1C} and therefore are suitable for analyzing the JM-targeting mechanism of α_{1C} [17]. Using this system, we for the first time identified the JM-targeting motif of α_{1C} and demonstrated that it is distinct from the previously identified membrane-targeting motif.

Interestingly the JM-targeting motif of α_{1C} is also different from that of α_{1S} [14]. The JM-targeting motif of α_{1S} corresponds to the amino acids residues 1735–1791 of α_{1C}. Since we found that the HA-$\alpha_{1C}\Delta$1733 mutant was normally clustered (Fig. 2), amino acid residues 1735–1791 are not necessary for the JM-targeting of α_{1C}. On the other hand, the JM-targeting motif of α_{1C} (amino acid residues 1681–1700) corresponds to residues 1555-1575 of α_{1S}. In our previous study, substitution of this region of α_{1S} with the corresponding part of α_{1A} did not affect the JM-targeting rate of α_{1S} [14]. Thus, although both α_{1S} and α_{1C} are similarly targeted to JM in GLT myotubes, their JM-targeting mechanism appears to be different.

Expression of α_{1C} restored action-potential induced Ca^{2+} transients triggered by CICR. With two α_{1C} channels possessing mutations in the JM-targeting motif the probability of CICR restoration was significantly decreased compared with WT α_{1C} channels (Fig. 6B). However, the reduction in the number of responsive cells by these mutations (i.e. ~60%) was much lower than that in their respective JM-targeting rate (i.e. ~90% in HA-α_{1C}1685AAAA1688 and 100% in HA-α_{1C}1666–1733$_A$, GFP-α_{1A} and GFP-α_{1A}CT$_C$ (Table 1)). This indicates that some of the α_{1C}- but not α_{1A}-based channels are still functionally coupled with RyR even though JM-targeting was below detectablility. Apparently, JM-targeting is not an all-or-non process and Ca^{2+} recording is somewhat more sensitive in detecting channels coupled to RyR than immunofluorescence analysis. This is to be expected if individual rather than clustered channels are coupled to RyR. Immunocytochemical study showed that the clustering rates of the tested mutants were paralleled with the pixel based LTCC-RyR colocalization index (Figs. 2 and 3), suggesting a good correlation between the channel clustering and colocalization with RyR. However, we could not assess the exact percentage of channel clusters colocalized with RyR. Therefore we cannot exclude the possibility that a minor fraction of non-clustered channels still functionally couples to RyR.

According to previous structural modeling of the C-terminus of α_{1C}, proximal (^{1681}LQAGLRTL^{1688}) and distal (^{1693}PEIRRAIS^{1700}) parts of the JM-targeting motif form two adjacent α-helices connected by a short loop [20]. Interestingly the distal helix of the motif overlaps with PCRD (amino acid residues 1694–1700)[20]. The distal C-terminal regulatory domain (DCRD) of the cleaved DCT reassociates with the PCRD of the truncated channel to auto-inhibit LTCC currents [10, 20]. This auto-inhibition plays a pivotal role in the response of LTCCs to β-adrenergic stimulation [21]. Fuller et al. also showed that in HEK cells Ba^{2+} currents of the truncated channel (Δ1800) were strongly inhibited by co-transfection of DCT at a molar ratio of DCT/channel higher than 0.75 [21]. We coexpressed DCT at various molar ratios with α_{1C} to examine whether the interaction of PCRD

and DCRD might compete with the JM-targeting of α_{1C}. However, the coexpression did not affect the JM-targeting rates of either full-length α_{1C} or truncated α_{1C} (α_{1C} Δ1821) in any conditions tested (Fig. 5). Our alanine scanning indicated that the proximal helix of the JM-targeting motif is more important for JM-targeting than the distal helix (Fig. 3). On the other hand, DCRD interacts with arginine 1696 and 1697 in distal helix of the PCRD [20]. Therefore, putative protein-protein interactions involving the JM-targeting motif and the PCRD-DCRD interaction may be mediated by closely adjacent but still distinct amino acids in the proximal C-terminus of α_{1C} subunit. These results indicate that the JM-targeting of α_{1C} and the responsiveness of LTCCs to PKA may not be mutually exclusive. This fact is important in light of the essential role of β-adrenergic augmentation of LTCC currents within cardiac dyad and peripheral junctions in the flight-or-fight response of animals.

Several proteins bind directly to the C-terminus of α_{1C}. In cardiac myocytes these include A-kinase anchoring protein 15 (AKAP15)[30], protein phosphatase 2A (PP2A)[31, 32], protein phosphatase 2B (PP2B, as known as calcineurin)[33], CaM [27, 28, 34-37] and sorcin [29, 38, 39]. Among these, AKAP15, PP2A, and PP2B interact with the cleaved DCT. Because the deletion mutants lacking the DCT (α_{1C}Δ1821 and α_{1C}Δ1733) were normally targeted into JM, these proteins are probably not involved in JM-targeting of α_{1C}. CaM and sorcin bind to the C-terminal segment close to the JM-targeting motif of α_{1C}. However, coexpression of CaM, CaM_{1234}, and sorcin with GFP-α_{1C} did not alter the JM-targeting of α_{1C} (Fig. S3), indicating that excess CaM and sorcin does not affect the function of the JM-targeting motif of α_{1C}. On the other hands, it has been reported that association of α_{1C} with CaM is involved in membrane trafficking of α_{1C} in hippocampal neurons and HEK293 cell [37]. Thus, it is possible that endogenous CaM also participates in the JM-targeting of α_{1C} in myotubes. Future studies such as knockdown of CaM and/or sorcin will be needed to clarify the requirements of endogenous CaM and sorcin for the JM-targeting of α_{1C}.

The most straightforward interpretation of our results would be that the JM-targeting motif significantly contributes to a protein-protein interaction that supports the JM-targeting of α_{1C}. However, addition of the JM-targeting motif to CD8 or α_{1A} was not sufficient for the targeting of these proteins to JM (Fig. 4). This may indicate that the motif identified in this study is not the actual protein-protein binding site. Alternatively, the insufficiency of the motif in JM-targeting may indicate that parts of α_{1C} other than the identified targeting motif contribute to JM-targeting. For instance, mutation or deletion of this motif might disrupt the structure and/or folding of other parts of α_{1C} meditating the JM-targeting and thus secondarily impair the targeting of α_{1C}. However, our results of the C-terminal deletion mutants and chimeras (Fig. 2) exclude the possibility that parts of the C-terminus other than the JM-targeting motif are necessary for the targeting. Furthermore it is unlikely that either of the N-terminus, I-II, II-III, and the III-IV loop is required for JM-targeting because their substitution with the corresponding sequences of α_{1A} did not disrupt the JM-targeting (Fig. 1). Apparently JM-targeting is a complex mechanism that necessitates the overall structure of the LTCC channel family. Indeed, a hemi-α_{1S} channel composed of III-IV domains and the C-terminus including the JM-targeting motif by itself was not targeted to JM, but JM-targeting was restored when it was coexpressed with the corresponding I-II hemi-channel [40].

To summarize, the results of this study for the first time identified the sequence motif in the proximal C-terminus of α_{1C} that is necessary for the JM-targeting of this LTCCs in muscle cells. The mutations in the JM-targeting motif of α_{1C} significantly impaired the efficiency of α_{1C}-induced restoration of EC coupling in GLT myotube. Because this motif is necessary but not sufficient for JM targeting of α_{1C}, further studies will be necessary to identify additional structural elements that contribute to the targeting function. Moreover it is important to identify the putative binding partner of the motif to reveal the molecular mechanism underlying efficient EC coupling of cardiac myocytes and its derangement in heart failure.

AUTHOR CONTRIBUTION

Tsutomu Nakada, Bernhard E. Flucher, and MitsuhikoYamada designed the research, analysed the data and wrote the paper. Tsutomu Nakada, Toshihide Kashihara, Xiaona Sheng, Toshihide Shibazaki, Miwa Horiuchi-Hirose, Simmon Gomi, and Masamichi Hirose performed the experiments.

ACKNOWLEDGMENTS

We are grateful to Prof. William Catterall (University of Washington) and Prof. Manfred Grabner (Innsbruck Medical University) for kindly providing the cDNA of α_1 subunits. We are grateful to Dr. Nagomi Kurebayashi (Juntendo University School of Medicine) for helpful advice on cytosolic Ca^{2+} measurement. We are grateful to Ms. Reiko Sakai for her secretarial assistance.

FUNDING

This work was supported by Grants-in-aid for Scientific Research 22790206 from the Ministry of Education, Culture, Sport, Science and Technology of Japan (MEXT), Medical Scientific Research from Shinshu Foundation for Promotion of Medical Sciences, a Sakakibara Memorial Research Grant from the Japan Research Promotion Society for Cardiovascular Diseases, and the Takeda Science Foundation to TN., by a grant-in-aid for Scientific Research 21590275 from the Japan Society for the Promotion of Sciences (JSPS) to MY., and by a grant from the Austrian Science Fund (FWF P23479-B19) to BEF.

REFERENCES

1. Catterall, W.A. (1994) Molecular properties of a superfamily of plasma-membrane cation channels. Curr. Opin. Cell. Biol. **6**, 607-615
2. Snutch, T.P. and Reiner, P.B. (1992) Ca^{2+} channels: diversity of form and function. Curr. Opin. Neurobiol. **2**, 247-253
3. Arikkath, J. and Campbell, K.P. (2003) Auxiliary subunits: essential components of the voltage-gated calcium channel complex. Curr. Opin. Neurobiol. **13**, 298-307
4. Tanabe, T., Takeshima, H., Mikami, A., Flockerzi, V., Takahashi, H., Kangawa, K., Kojima, M., Matsuo, H., Hirose, T. and Numa, S. (1987) Primary structure of the receptor for calcium channel blockers from skeletal muscle. Nature **328**, 313-318
5. Carl, S.L., Felix, K., Caswell, A.H., Brandt, N.R., Ball, W.J.J., Vaghy, P.L., Meissner, G. and Ferguson, D.G. (1995) Immunolocalization of sarcolemmal dihydropyridine receptor and sarcoplasmic reticular triadin and ryanodine receptor in rabbit ventricle and atrium. J. Cell Biol. **129**, 673-682
6. Flucher, B.E., Morton, M.E., Froehner, S.C. and Daniels, M.P. (1990) Localization of the α_1 and α_2 subunits of the dihydropyridine receptor and ankyrin in skeletal muscle triads. Neuron **5**, 339-351
7. Jorgensen, A.O., Shen, A.C., Arnold, W., Leung, A.T. and Campbell, K.P. (1989) Subcellular distribution of the 1,4-dihydropyridine receptor in rabbit skeletal muscle in situ: an immunofluorescence and immunocolloidal gold-labeling study. J. Cell. Biol. **109**, 135-147
8. Cannell, M.B. and Soeller, C. (1997) Numerical analysis of ryanodine receptor activation by L-type channel activity in the cardiac muscle diad. Biophys. J. **73**, 112-122
9. Fabiato, A. (1985) Time and calcium dependence of activation and inactivation of calcium-induced release of calcium from the sarcoplasmic reticulum of a skinned canine cardiac Purkinje cell. J. Gen. Physiol. **85**, 247-289
10. Gao, T., Bunemann, M., Gerhardstein, B.L., Ma, H. and Hosey, M.M. (2000) Role of the C terminus of the α_{1C} ($Ca_V1.2$) subunit in membrane targeting of cardiac L-type calcium channels. J. Biol. Chem. **275**, 25436-25444
11. Suda, N., Franzius, D., Fleig, A., Nishimura, S., Bodding, M., Hoth, M., Takeshima, H. and Penner, R. (1997) Ca^{2+}-induced Ca^{2+} release in Chinese hamster ovary (CHO) cells co-expressing dihydropyridine and ryanodine receptors. J. Gen. Physiol. **109**, 619-631
12. Takekura, H., Takeshima, H., Nishimura, S., Takahashi, M., Tanabe, T., Flockerzi, V., Hofmann, F. and Franzini-Armstrong, C. (1995) Co-expression in CHO cells of two muscle proteins involved in excitation-contraction coupling. J. Muscle. Res. Cell Motil. **16**, 465-480
13. Powell, J.A., Petherbridge, L. and Flucher, B.E. (1996) Formation of triads without the dihydropyridine receptor alpha subunits in cell lines from dysgenic skeletal muscle. J Cell Biol **134**, 375-387
14. Flucher, B.E., Kasielke, N. and Grabner, M. (2000) The triad targeting signal of the skeletal muscle calcium channel is localized in the COOH terminus of the α_{1S} subunit. J. Cell. Biol. **151**, 467-478
15. Grabner, M., Dirksen, R.T. and Beam, K.G. (1998) Tagging with green fluorescent protein reveals a distinct subcellular distribution of L-type and non-L-type Ca^{2+} channels expressed in dysgenic myotubes. Proc Natl Acad Sci U S A **95**, 1903-1908
16. Takekura, H., Paolini, C., Franzini-Armstrong, C., Kugler, G., Grabner, M. and Flucher, B.E. (2004) Differential contribution of skeletal and cardiac II-III loop sequences to the assembly of dihydropyridine-receptor arrays in skeletal muscle. Mol. Biol. Cell **15**, 5408-5419
17. Tuluc, P., Kern, G., Obermair, G.J. and Flucher, B.E. (2007) Computer modeling of siRNA knockdown effects indicates an essential role of the Ca^{2+} channel $\alpha_2\delta$-1 subunit in cardiac excitation-contraction coupling. Proc. Natl. Acad. Sci. U. S. A. **104**, 11091-11096
18. Gao, T., Puri, T.S., Gerhardstein, B.L., Chien, A.J., Green, R.D. and Hosey, M.M. (1997)

Identification and subcellular localization of the subunits of L-type calcium channels and adenylyl cyclase in cardiac myocytes. J. Biol. Chem. **272**, 19401-19407
19. Gao, T., Cuadra, A.E., Ma, H., Bunemann, M., Gerhardstein, B.L., Cheng, T., Eick, R.T. and Hosey, M.M. (2001) C-terminal fragments of the α_{1C} ($Ca_V1.2$) subunit associate with and regulate L-type calcium channels containing C-terminal-truncated α_{1C} subunits. J. Biol. Chem. **276**, 21089-21097
20. Hulme, J.T., Yarov-Yarovoy, V., Lin, T.W., Scheuer, T. and Catterall, W.A. (2006) Autoinhibitory control of the $Ca_V1.2$ channel by its proteolytically processed distal C-terminal domain. J. Physiol. **576**, 87-102
21. Fuller, M.D., Emrick, M.A., Sadilek, M., Scheuer, T. and Catterall, W.A. (2010) Molecular mechanism of calcium channel regulation in the fight-or-flight response. Sci. Signal. **3**, ra70
22. Horton, R.M., Hunt, H.D., Ho, S.N., Pullen, J.K. and Pease, L.R. (1989) Engineering hybrid genes without the use of restriction enzymes: gene splicing by overlap extension. Gene **77**, 61-68
23. Altier, C., Dubel, S.J., Barrere, C., Jarvis, S.E., Stotz, S.C., Spaetgens, R.L., Scott, J.D., Cornet, V., De Waard, M., Zamponi, G.W., Nargeot, J. and Bourinet, E. (2002) Trafficking of L-type calcium channels mediated by the postsynaptic scaffolding protein AKAP79. J. Biol. Chem. **277**, 33598-33603
24. Di Biase, V., Obermair, G.J., Szabo, Z., Altier, C., Sanguesa, J., Bourinet, E. and Flucher, B.E. (2008) Stable membrane expression of postsynaptic $Ca_V1.2$ calcium channel clusters is independent of interactions with AKAP79/150 and PDZ proteins. J. Neurosci. **28**, 13845-13855
25. Kasielke, N., Obermair, G.J., Kugler, G., Grabner, M. and Flucher, B.E. (2003) Cardiac-type EC-coupling in dysgenic myotubes restored with Ca^{2+} channel subunit isoforms α_{1C} and α_{1D} does not correlate with current density. Biophys. J. **84**, 3816-3828
26. Grabner, M., Bachmann, A., Rosenthal, F., Striessnig, J., Schultz, C., Tautz, D. and Glossmann, H. (1994) Insect calcium channels. Molecular cloning of an α_1-subunit from housefly (Musca domestica) muscle. FEBS Lett. **339**, 189-194
27. Peterson, B.Z., DeMaria, C.D., Adelman, J.P. and Yue, D.T. (1999) Calmodulin is the Ca^{2+} sensor for Ca^{2+} -dependent inactivation of L-type calcium channels. Neuron **22**, 549-558
28. Zuhlke, R.D., Pitt, G.S., Deisseroth, K., Tsien, R.W. and Reuter, H. (1999) Calmodulin supports both inactivation and facilitation of L-type calcium channels. Nature **399**, 159-162
29. Meyers, M.B., Puri, T.S., Chien, A.J., Gao, T., Hsu, P.H., Hosey, M.M. and Fishman, G.I. (1998) Sorcin associates with the pore-forming subunit of voltage-dependent L-type Ca^{2+} channels. J. Biol. Chem. **273**, 18930-18935
30. Hulme, J.T., Lin, T.W., Westenbroek, R.E., Scheuer, T. and Catterall, W.A. (2003) Beta-adrenergic regulation requires direct anchoring of PKA to cardiac $Ca_V1.2$ channels via a leucine zipper interaction with A kinase-anchoring protein 15. Proc. Natl. Acad. Sci. U. S. A. **100**, 13093-13098
31. Davare, M.A., Horne, M.C. and Hell, J.W. (2000) Protein phosphatase 2A is associated with class C L-type calcium channels (Cav1.2) and antagonizes channel phosphorylation by cAMP-dependent protein kinase. J. Biol. Chem. **275**, 39710-39717
32. Hall, D.D., Feekes, J.A., Arachchige Don, A.S., Shi, M., Hamid, J., Chen, L., Strack, S., Zamponi, G.W., Horne, M.C. and Hell, J.W. (2006) Binding of protein phosphatase 2A to the L-type calcium channel Cav1.2 next to Ser1928, its main PKA site, is critical for Ser1928 dephosphorylation. Biochemistry **45**, 3448-3459
33. Xu, H., Ginsburg, K.S., Hall, D.D., Zimmermann, M., Stein, I.S., Zhang, M., Tandan, S., Hill, J.A., Horne, M.C., Bers, D. and Hell, J.W. (2010) Targeting of protein phosphatases PP2A and PP2B to the C-terminus of the L-type calcium channel Cav1.2. Biochemistry **49**, 10298-10307
34. Erickson, M.G., Liang, H., Mori, M.X. and Yue, D.T. (2003) FRET two-hybrid mapping reveals function and location of L-type Ca^{2+} channel CaM preassociation. Neuron **39**, 97-107
35. Pate, P., Mochca-Morales, J., Wu, Y., Zhang, J.Z., Rodney, G.G., Serysheva, I.I., Williams, B.Y.,

Anderson, M.E. and Hamilton, S.L. (2000) Determinants for calmodulin binding on voltage-dependent Ca^{2+} channels. J. Biol. Chem. **275**, 39786-39792
36. Pitt, G.S., Zuhlke, R.D., Hudmon, A., Schulman, H., Reuter, H. and Tsien, R.W. (2001) Molecular basis of calmodulin tethering and Ca^{2+}-dependent inactivation of L-type Ca^{2+} channels. J. Biol. Chem. **276**, 30794-30802
37. Wang, H.G., George, M.S., Kim, J., Wang, C. and Pitt, G.S. (2007) Ca^{2+}/calmodulin regulates trafficking of $Ca_V1.2$ Ca^{2+} channels in cultured hippocampal neurons. J. Neurosci. **27**, 9086-9093
38. Fowler, M.R., Colotti, G., Chiancone, E., Smith, G.L. and Fearon, I.M. (2008) Sorcin modulates cardiac L-type Ca^{2+} current by functional interaction with the alpha1C subunit in rabbits. Exp. Physiol. **93**, 1233-1238
39. Fowler, M.R., Colotti, G., Chiancone, E., Higuchi, Y., Seidler, T. and Smith, G.L. (2009) Complex modulation of L-type Ca^{2+} current inactivation by sorcin in isolated rabbit cardiomyocytes. Pflugers Arch. **457**, 1049-1060
40. Flucher, B.E., Weiss, R.G. and Grabner, M. (2002) Cooperation of two-domain Ca^{2+} channel fragments in triad targeting and restoration of excitation- contraction coupling in skeletal muscle. Proc. Natl. Acad. Sci. U. S. A. **99**, 10167-10172

Table 1 *JM-targeting rate of each construct.*
Each expression vector was transiently transfected into GLT cells, and expressed proteins were detected by anti-GFP, anti-HA or anti-CD8 antibodies. To detect proteins only expressed properly in plasma membranes, anti-HA and anti-CD8 antibodies were reacted without membrane permeabilization by detergent. For each construct, 3-5 coverslips (40-205 myotubes/coverslip) were tested to obtain means ± S.E.M. The *asterisk* and *sharp* indicate a significant difference ($p < 0.01$) versus GFP-α_{1C} and HA-α_{1C}, respectively. "No" indicates no membrane targeting.

Constructs	Percent of cells with clusters (means ± S.E.M)	Total cell number
GFP-α_{1C}	56.8 ± 4.1	375
GFP-α_{1A}	0*	231
GFP-$\alpha_{1C}NT_A$	50.5 ± 2.9	303
GFP-$\alpha_{1C}I\text{-}II_A$	49.6 ± 8.0	277
GFP-$\alpha_{1C}II\text{-}III_M$	43.5 ± 2.2*	296
GFP-$\alpha_{1C}III\text{-}IV_A$	13.4 ± 0.5*	297
GFP-$\alpha_{1C}CT_A$	0*	327
HA-α_{1C}	91.7 ± 0.3	300
HA-$\alpha_{1C}\Delta1821$	76.4 ± 3.9#	316
HA-$\alpha_{1C}\Delta1733$	87.3 ± 3.1	294
HA-$\alpha_{1C}\Delta1666$	0#	407
HA-$\alpha_{1C}\Delta1624$	No	289
HA-$\alpha_{1C}1507–1650_A$	80.2 ± 5.6#	330
HA-$\alpha_{1C}1624–1665_A$	80.0 ± 5.4#	233
HA-$\alpha_{1C}1666–1733_A$	0#	324
HA-$\alpha_{1C}1666–1676_A$	79.7 ± 3.2#	302
HA-$\alpha_{1C}1666–1688_A$	1.1 ± 0.6#	232
HA-$\alpha_{1C}1689–1733_A$	2.8 ± 1.1#	285
HA-$\alpha_{1C}1709–1733_A$	90.3 ± 1.5	321
HA-α_{1C}1677AAAA1680	89.0 ± 2.3	300
HA-α_{1C}1681AAAA1684	11.7 ± 0.9#	300
HA-α_{1C}1685AAAA1688	6.7 ± 2.2#	300
HA-α_{1C}1689AAAA1692	78.3 ± 2.9#	300
HA-α_{1C}1693AAAA1696	59.7 ± 1.7#	300
HA-α_{1C}1697AAAA1700	24.0 ± 5.0#	300
HA-α_{1C}1701AAAA1704	86.3 ± 0.3	300
HA-α_{1C}1705AAAA1708	85.7 ± 0.9	300
CD8-α_{1C}CT	0	281
GFP-$\alpha_{1A}JMT_C$	0	290
GFP-$\alpha_{1A}CT_C$	0	312
HA-α_{1C} + mock	86.1 ± 1.6	319
HA-α_{1C} + CaM_{WT}	83.0 ± 2.3	325
HA-α_{1C} + CaM_{1234}	78.8 ± 6.9	301
HA-α_{1C} + sorcin	79.0 ± 3.8	328
HA-$\alpha_{1C}\Delta1821$	88.8 ± 4.0	294
HA-$\alpha_{1C}\Delta1821$+ DCT (1:0.8)	87.1 ± 2.2	307
HA-$\alpha_{1C}\Delta1821$+ DCT (1:1.6)	85.7 ± 2.1	296
HA-$\alpha_{1C}\Delta1821$+ DCT (1:3.2)	82.6 ± 2.5	310
HA-$\alpha_{1C}\Delta1821$+ mock (1:0.8)	88.2 ± 1.1	295

HA-α_{1C}Δ1821+ mock (1:1.6)	87.0 ± 2.3	309
HA-α_{1C}Δ1821+ mock (1:3.2)	90.3 ± 2.0	432
HA-α_{1C} + DCT (1:0.8)	90.7 ± 1.6	321
HA-α_{1C} + DCT (1:1.6)	86.1 ± 1.6	268
HA-α_{1C} + DCT (1:3.2)	84.6 ± 2.5	261

FIGURE LEGENDS

Fig. 1. Localization of the JM-targeting motif in the C-terminus of α_{1C}.
A, Schematic representation of chimeric constructs. Cytosolic domains of α_{1C} were substituted with corresponding regions of α_{1A} (N-terminus, I-II loop, III-IV loop, C-terminus) or α_{1M} (II-III loop). Bold lines indicate substituted region in each chimera. All chimeras are N-terminal GFP fusion constructs. *B*, *C*, Failure of the C-terminal chimera to be targeted to JM. Transfected WT channels and chimeras were immuno-localized with anti-GFP and Alexa 488-labeled secondary antibody (*upper panels, green* in merged view) using a confocal microscope. JM was labeled with anti-RyR and Alexa 555-labeled secondary antibody (*middle panels, red* in merged view). Merged color images (*bottom panels*) with nuclei stained with Hoechst 33342 (*blue*). Bar = 10 μm.

Fig. 2. Identification of the JM-targeting motif in the proximal part of the C-terminus of α_{1C}.
A, Schematic representing the last transmembrane segment (IVS6) and the C-terminus of deletion mutants and chimeras based on α_{1C}. Black and white bars represent amino acid sequence derived from α_{1C} and α_{1A}, respectively. Plus (+) and minus (–) symbols at right indicate the JM-targeting properties of each mutant in GLT myotubes. *B*, Representative confocal images showing distributions of JM-targeted- (HA-α_{1C}) and not JM-targeted- (HA-$\alpha_{1C}\Delta$1666) channels in GLT myotubes. Wild type and deletion mutants expressed in the plasma membrane were detected with anti-HA and alexa-555 labeled secondary antibody (*left panels*, *red* in merged view) without membrane permeabilization. RyR was detected with anti-RyR and alexa-488 labeled secondary antibody (*center panels*, *green* in merged view). Merged color images (*right panels*) with nuclei stained with Hoechst 33342 (*blue*). Enlarged views of the regions enclosed by white frames are shown in insets. Bar = 20 μm. *C*, Confocal images showing that deletion or substitution of the proximal part in C-terminus of α_{1C} affected JM-targeting. Mutants and chimeras expressed in the plasma membrane were detected with anti-HA and alexa-555 labeled secondary antibody without membrane permeabilization. Enlarged views of the regions enclosed by white frames are shown in insets. Bar = 20 μm. *D*, Colocalization of mutant channels and RyR in myotubes. Colocalization of mutant channels (labeled with anti-HA antibody) with RyR (labeled with anti-RyR antibody) was calculated from images of 10-12 myotubes in each group. Values are the means ± S.E.M. The *asterisk* indicates a significant difference ($p < 0.01$) versus WT.

Fig. 3. Alanine substitution of the JM-targeting motif in the C-terminus of α_{1C}.
A, Representative confocal images showing distributions of JM-targeted- (HA-α_{1C}1677AAAA1680) and not JM-targeted- (HA-α_{1C}1685AAAA1688) channels in GLT myotubes. Alanine substitution mutants expressed in the plasma membrane were detected with anti-HA and alexa-555 labeled secondary antibody (*left panels*, *red* in merged view) without membrane permeabilization. RyR was detected with anti-RyR and alexa-488 labeled secondary antibody (*center panels*, *green* in merged view). Merged color images (*right panels*) with nuclei stained with Hoechst 33342 (*blue*). Enlarged views of the regions enclosed by white frames are shown in insets. Bar = 20 μm. *B*, The percentage of myotubes with clustered distribution of WT and alanine substitution mutant of α_{1C}, indicating correct JM-targeting, was calculated. Four consecutive amino acid residues in the sequence identified as the JM-targeting motif were sequentially substituted with alanines. Values are the means ± S.E.M. The *asterisk* indicates a significant difference ($p < 0.01$) versus WT. *C*, Colocalization of the alanine substitution mutant channels and RyR in myotubes. Colocalization of mutant channels as used in *B* (labeled with anti-HA antibody) with RyR (labeled with anti-RyR antibody) was calculated from images of 10 myotubes in each group. Values are the means ± S.E.M. The *asterisk* indicates a significant difference ($p < 0.01$) versus WT.

Fig. 4. The C-terminus of α_{1C} is not sufficient for JM-targeting.
CD8-α_{1C}CT: the C-terminus of α_{1C} was fused to the C-terminus of CD8. GFP-$\alpha_{1A}CT_C$: the whole

C-terminus of GFP-α_{1A} was substituted with the C-terminus of α_{1C}. GFP-α_{1A}JMT$_C$: the proximal portion of C-terminus of α_{1A} was substituted with the JM-targeting motif of α_{1C}. These proteins were transiently expressed in GLT myotubes. The chimeric proteins were detected with anti-CD8 or anti-GFP antibodies and visualized with an Alexa 488-labeled secondary antibody (*left panels*, *green* in merged view). JM was labeled with anti-RyR and Alexa 555-labeled secondary antibody (*center panels*, *red* in merged view). Merged color images (*right panels*) with nuclei stained with Hoechst 33342 (*blue*). Bar = 20 μm.

Fig. 5. Effect of coexpression of distal C-terminal domain on JM-targeting motif of α_{1C}.
A, DCT of α_{1C} with N-terminal 3×FLAG-tag (*top panels, red* in merged view) was cotransfected with HA-$\alpha_{1C}\Delta$1821 or HA-α_{1C} (*middle panels, green* in merged view) in GLT myotubes. Merged color images with nuclei stained with Hoechst 33342 (*bottom panels, blue*). Bar = 20 μm. *B*, Percentages of myotubes with clustered distribution of HA-$\alpha_{1C}\Delta$1821 or HA-α_{1C}. Plasmid vectors coding for channels (HA-$\alpha_{1C}\Delta$1821 or HA-α_{1C}) and DCT were co-transfected with various molar ratios in the GLT myotube. Plus (+) and minus (–) symbols indicate the transfection of each vector. Wedges indicate increasing amounts of DCT or mock vectors transfected (DCT/channel vectors molar ratios were 0.8, 1.6, and 3.2).

Fig. 6. Action potential-elicited Ca^{2+} transient in GLT myotubes expressing wild-type and mutant α_{1C}.
A. Representative traces of action potential- and caffeine-induced Ca^{2+} transients in myotubes transfected with HA-α_{1C}, HA-α_{1C}1685AAAA1688 or HA-α_{1C}1666–1733$_A$. Electrical field stimulation (50 V, 1 ms, 0.3 Hz as marked) evoked Ca^{2+} transients in myotubes expressing HA-α_{1C} (*upper* panel) and HA-α_{1C}1685AAAA1688 (*middle* panel), and HA-α_{1C}1666–1733$_A$ (*lower* panel). To block the Ca^{2+} influx during the stimulation, 0.5 mM Cd^{2+}/0.1 mM La^{3+} was extracellularly applied. Subsequently, 6 mM caffeine was rapidly applied to the bath to completely release Ca^{2+} from the SR. *B*. Myotubes responding to field stimulation were counted. Counts from eight experiments are expressed as the percentage (means ± S.E.M.) of the averaged value for HA-α_{1C}. The *asterisk* indicates a significant difference ($p < 0.05$) versus WT. *C*. Myotubes expressing the transfected channels were counted. Cultures were stained with anti-myosin heavy chain (for all culture, differentiation marker) and anti-HA (for HA-α_{1C}, HA-α_{1C}1685AAAA1688, and HA-α_{1C}1666–1733$_A$) or anti-GFP (GFP-α_{1A} and GFP-α_{1A}CT$_C$) antibodies. Low magnification (10x objective) fluorescence images were acquired from 5 randomly selected areas of each specimen, and the number of myotube expressing both channels and myosin heavy chains was quantified. Counts from three experiments are expressed as the percentage (means ± S.E.M.) of the averaged value for HA-α_{1C}.

Fig. 1

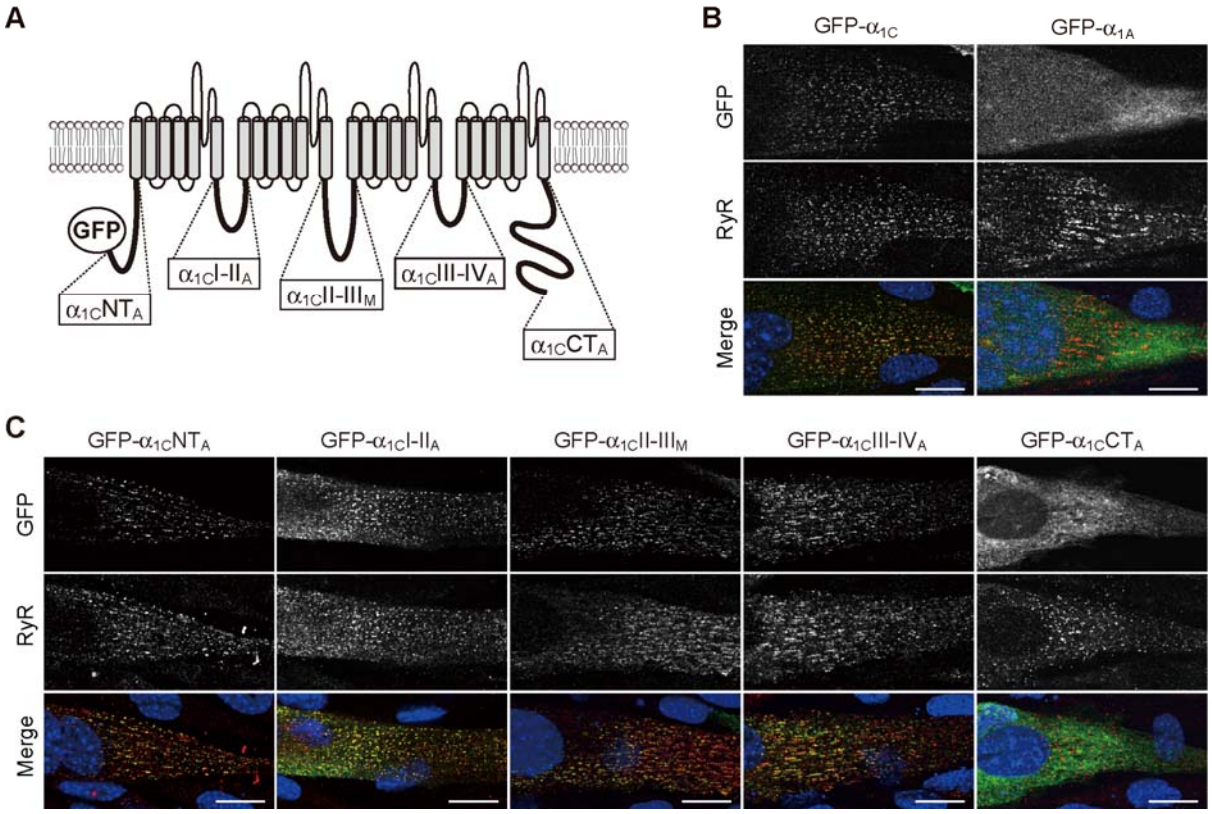
A
GFP
α_{1C}NT$_A$
α_{1C}I-II$_A$
α_{1C}II-III$_M$
α_{1C}III-IV$_A$
α_{1C}CT$_A$
B
GFP-α_{1C}
GFP-α_{1A}
GFP
RyR
Merge
C
GFP-α_{1C}NT$_A$
GFP-α_{1C}I-II$_A$
GFP-α_{1C}II-III$_M$
GFP-α_{1C}III-IV$_A$
GFP-α_{1C}CT$_A$
GFP
RyR
Merge

Fig. 2

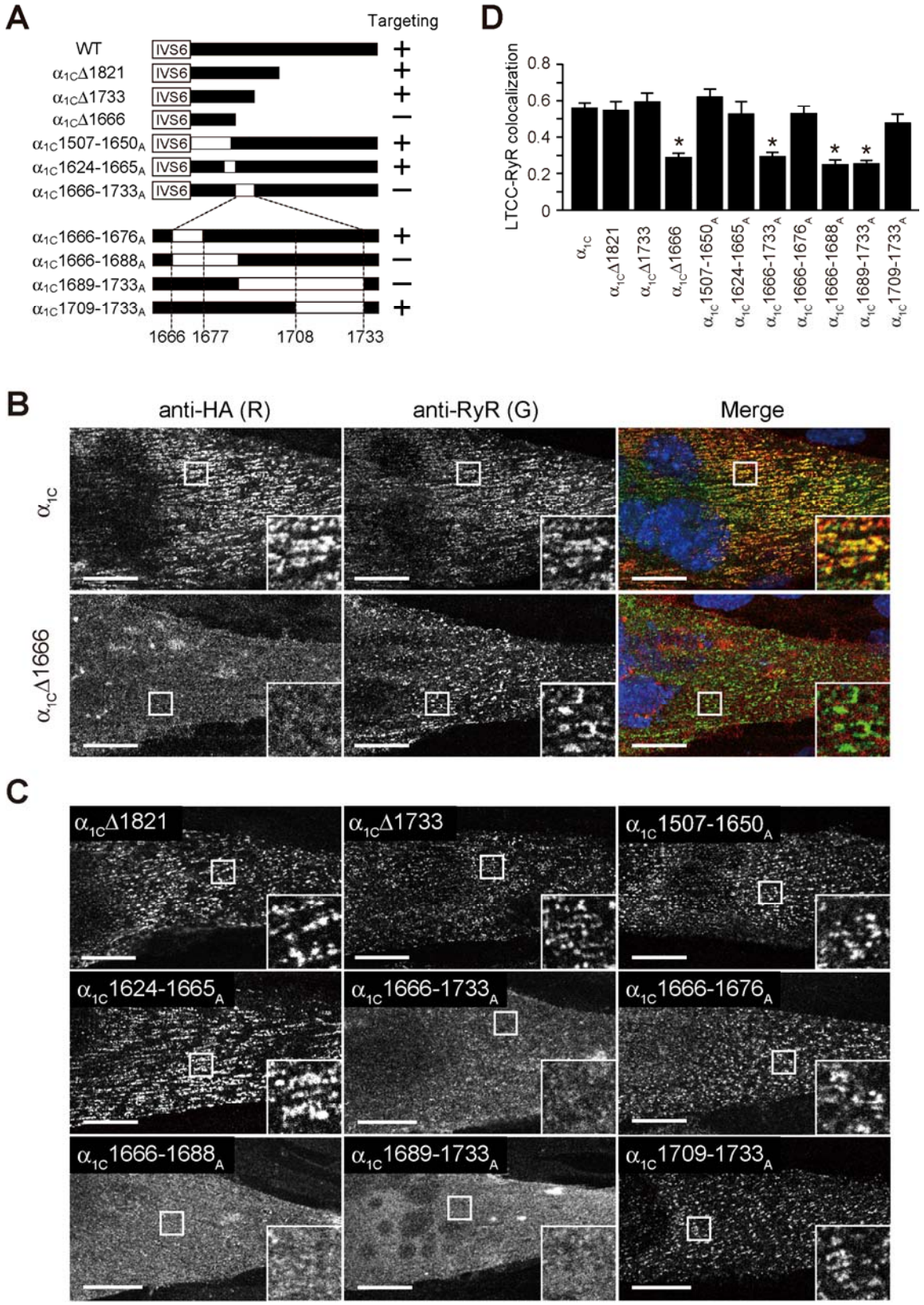
A
Targeting
WT
IVS6
α1CΔ1821
α1CΔ1733
α1CΔ1666
α1C1507-1650A
α1C1624-1665A
α1C1666-1733A
α1C1666-1676A
α1C1666-1688A
α1C1689-1733A
α1C1709-1733A
1666 1677 1708 1733
D
LTCC-RyR colocalization
0.8
0.6
0.4
0.2
0
α1C
α1CΔ1821
α1CΔ1733
α1CΔ1666
α1C1507-1650A
α1C1624-1665A
α1C1666-1733A
α1C1666-1676A
α1C1666-1688A
α1C1689-1733A
α1C1709-1733A
B
anti-HA (R)
anti-RyR (G)
Merge
α1C
α1CΔ1666
C
α1CΔ1821
α1CΔ1733
α1C1507-1650A
α1C1624-1665A
α1C1666-1733A
α1C1666-1676A
α1C1666-1688A
α1C1689-1733A
α1C1709-1733A

Fig. 3

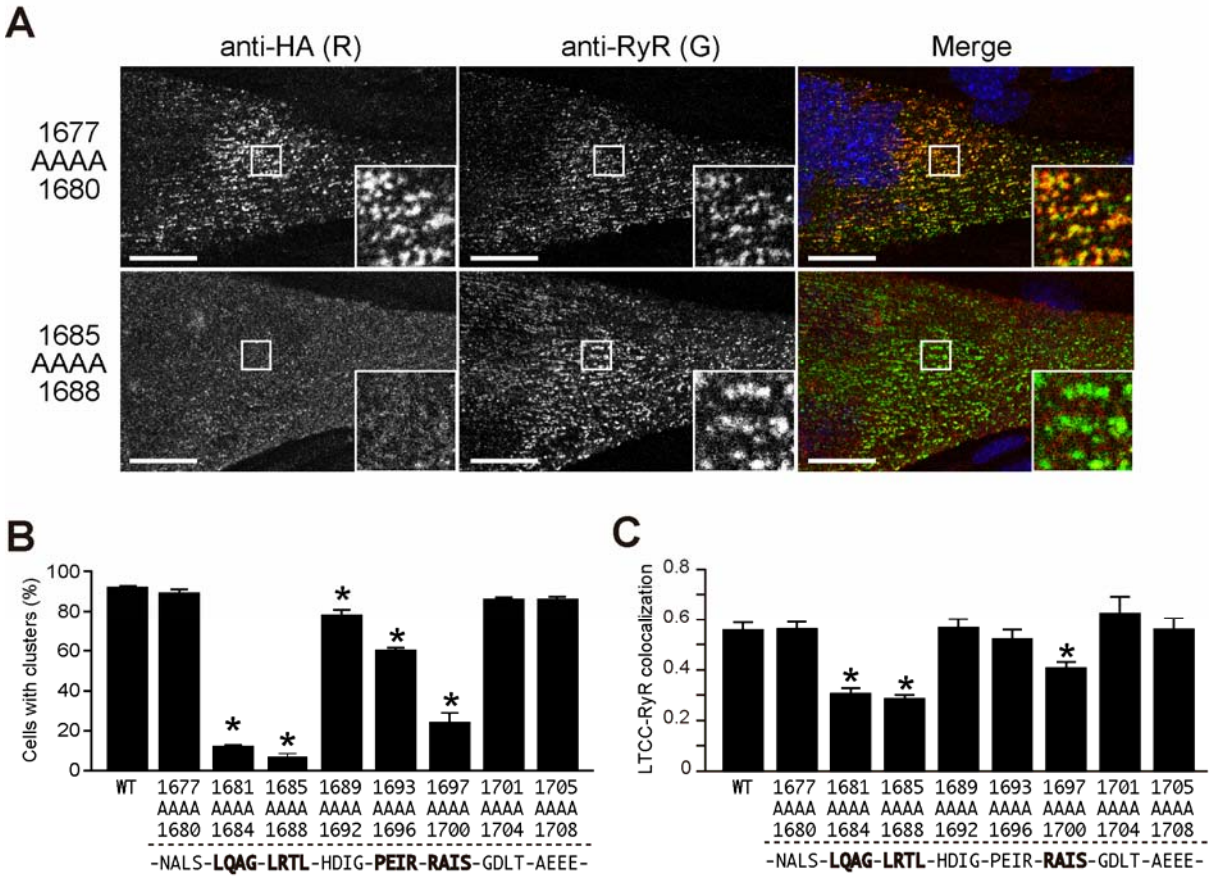
A
anti-HA (R)
anti-RyR (G)
Merge
1677
AAAA
1680
1685
AAAA
1688
B
Cells with clusters (%)
100
80
60
40
20
0
WT
1677 AAAA 1680
1681 AAAA 1684
1685 AAAA 1688
1689 AAAA 1692
1693 AAAA 1696
1697 AAAA 1700
1701 AAAA 1704
1705 AAAA 1708
-NALS-LQAG-LRTL-HDIG-PEIR-RAIS-GDLT-AEEE-
C
LTCC-RyR colocalization
0.8
0.6
0.4
0.2
0
WT
1677 AAAA 1680
1681 AAAA 1684
1685 AAAA 1688
1689 AAAA 1692
1693 AAAA 1696
1697 AAAA 1700
1701 AAAA 1704
1705 AAAA 1708
-NALS-LQAG-LRTL-HDIG-PEIR-RAIS-GDLT-AEEE-

Fig. 4

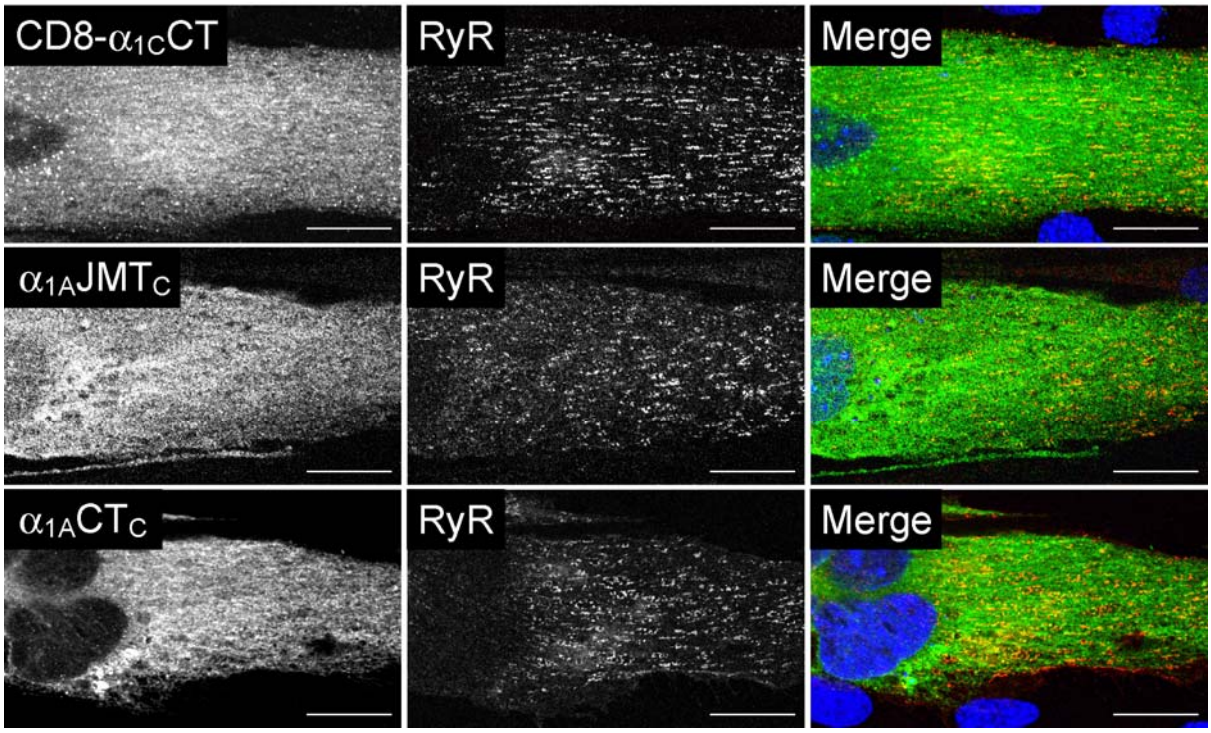

Fig. 5

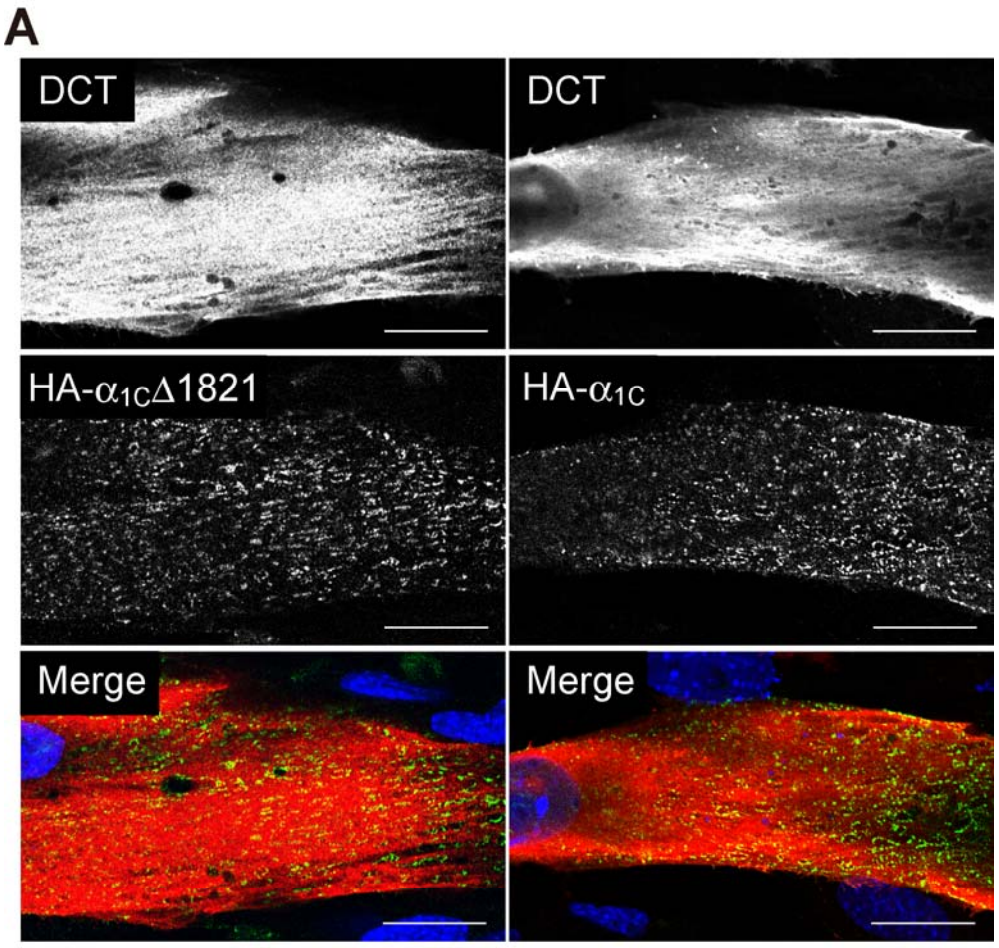
A
DCT
DCT
HA-α1CΔ1821
HA-α1C
Merge
Merge

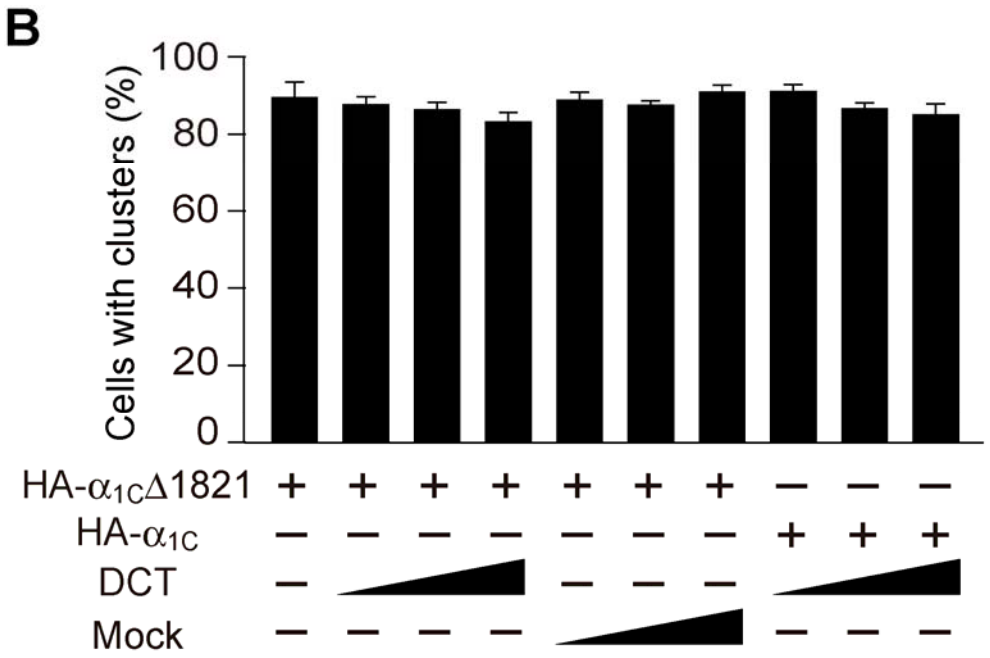
B
Cells with clusters (%)
100
80
60
40
20
0
HA-α1CΔ1821 + + + + + + + − − −
HA-α1C − − − − − − − + + +
DCT − − −
Mock − − −

Fig. 6

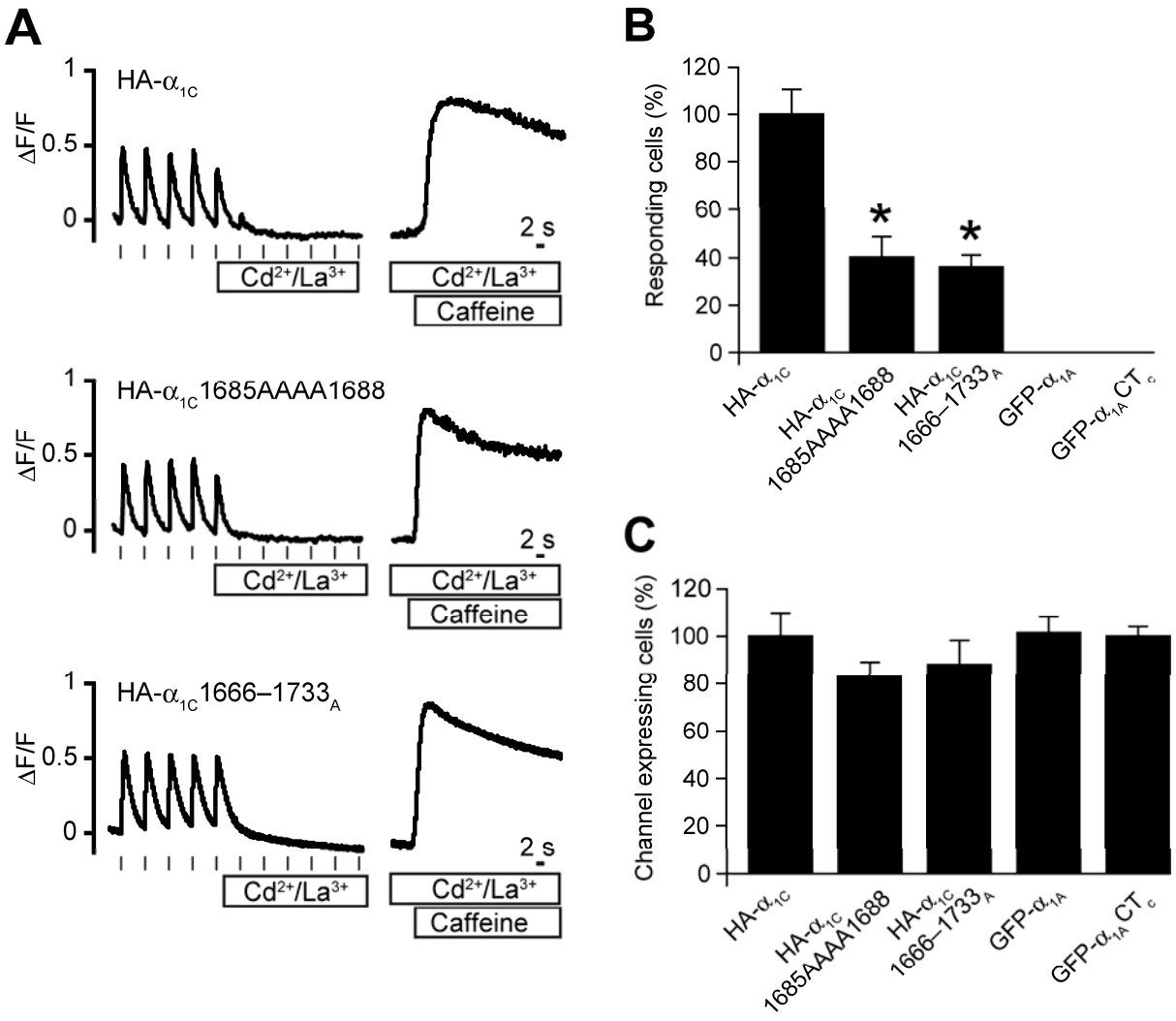
A
HA-α1C
ΔF/F
1
0.5
0
2 s
Cd2+/La3+
Cd2+/La3+
Caffeine
HA-α1C1685AAAA1688
HA-α1C1666–1733A
B
Responding cells (%)
120
100
80
60
40
20
0
*
*
HA-α1C
HA-α1C 1685AAAA1688
HA-α1C 1666–1733A
GFP-α1A
GFP-α1A CTc
C
Channel expressing cells (%)

SUPPLEMENTAL FIGURE LEGENDS

Figure S1. Detection of membrane-targeted channels in non-permeabilized myotubes.
Representative confocal images of JM-targeted (HA-α_{1C}), membrane-targeted but not JM-targeted (HA-$\alpha_{1C}\Delta$1666), and not membrane-targeted (HA-$\alpha_{1C}\Delta$1624) channels. Channels were detected with anti-HA antibody and alexa-555 labeled secondary antibody (*red*). Nuclei were stained with Hoechst 33342 (*blue*). All of the images in this figure were acquired with the same microscope and camera settings. Under non-permeabilized conditions, the photos show a clustered distribution of HA-α_{1C} (*a*), a diffuse and weak signal in plasma membranes of HA-$\alpha_{1C}\Delta$1666 (*b*), and no signal of HA-$\alpha_{1C}\Delta$1624 (*c*). Under permeabilized conditions, the clustered distribution of HA-α_{1C} was observed in ~20% of myotubes (*d*) whereas the remainder myotubes showed a ER/SR localization of HA-α_{1C} with strong fluorescence intensity probably due to the overexpression of the construct (*g*). Intense signals of HA-$\alpha_{1C}\Delta$1666 and HA-$\alpha_{1C}\Delta$1624 were also observed in the ER/SR system under the permeabilized condition (*e* and *f*). Under non-permeabilized conditions, no myotubes exhibited such intense signal as found in the permeabilized condition. Bar = 20 μm.

Figure S2. Expressions of HA-tagged channels in GLT myotubes.
Equal amounts of whole cell lysates from GLT myotubes transfected with individual HA-tagged channels were subjected to 5% SDS-PAGE and immunoblotted with anti-HA antibody.

Figure S3. Effect of coexpression of α_{1C}-binding proteins on JM-targeting motif of α_{1C}.
A, CaM_{WT}, CaM_{1234}, or sorcin with N-terminal 3×FLAG-tag were cotransfected with HA-α_{1C} in GLT myotubes. Plasma membrane-targeted HA-α_{1C} was detected with anti-HA without membrane permeabilization, and anti-FLAG antibody was applied after permeabilization to detect 3×FLAG-tagged proteins. Alexa 555- (for FLAG-tag, *red*) and 488- (for HA-tag, *green*) labeled secondary antibodies were used and nuclei were stained with Hoechst 33342 (*blue*). Bar = 20 μm. *B*, Percentages of myotubes with clustered distribution of HA-α_{1C} constructs. For each construct, three or four coverslips were analyzed, and at least 100 myotubes were counted per coverslip. Similar results were obtained in three independent experiments. Values are the means ± S.E.M.

Figure S4. Representative images used to quantify channel-expressing myotubes.
To assess the expression of each construct, the myotubes were transfected with HA-α_{1C}, HA-α_{1C}1685AAAA1688, HA-α_{1C}1666–1733_A, GFP-α_{1A}, or GFP-$\alpha_{1A}CT_C$ under an identical condition of the Ca^{2+} imaging experiments (Fig. 6). The cultures were stained with anti-HA (for HA-α_{1C}, HA-α_{1C}1685AAAA1688, and HA-α_{1C}1666–1733_A, *green* in merged view) or anti-GFP (for GFP-α_{1A} and GFP-$\alpha_{1A}CT_C$, *green* in merged view), and anti-myosin heavy chain (for all cultures, *red* in merged view). Hoechst 33342 was used to visualize the nuclei (*blue* in merged view). Low magnification (10x objective) fluorescence images were acquired, and quantified number of myotube expressed both channel and myosin heavy chain. The result of quantification was shown in Fig 6C. Bar = 200 μm.

SUPPLEMENTAL MATERIAL AND METHODS

Western blotting

GLT myotubes transfected with individual plasmids were lysed with Cell lysis buffer (Cell Signaling Technology, Danvers, MA) contained protease inhibitor cocktail (Roche Diagnostics). The protein concentrations of samples were measured by a BCA protein assay kit (Thermo Fisher Scientific). Equal amounts of samples were separated on 5% SDS-PAGE and electroblotted onto polyvinylidene difluoride membranes. Non-specific binding was blocked with 5% nonfat skim milk in TBST (150 mM NaCl, 100 mM Tris, and 0.1% Tween 20, pH 7.4) for 1 h at room temperature. Membranes were incubated with anti-HA rat monoclonal antibody (Roche Applied Science, clone 3F10, 1:2000) overnight at 4°C. After being washed with TBST, membranes were reacted with horseradish peroxidase-conjugated donkey anti-rat IgG (1:10,000, Jackson ImmunoResearch Laboratories, West Grove, PA) for 1 h at room temperature. The bound secondary antibody was visualized with ECL-Plus reagent (BD Biosciences, San Jose, CA) according to the manufacturer's instructions.

Fig. S1

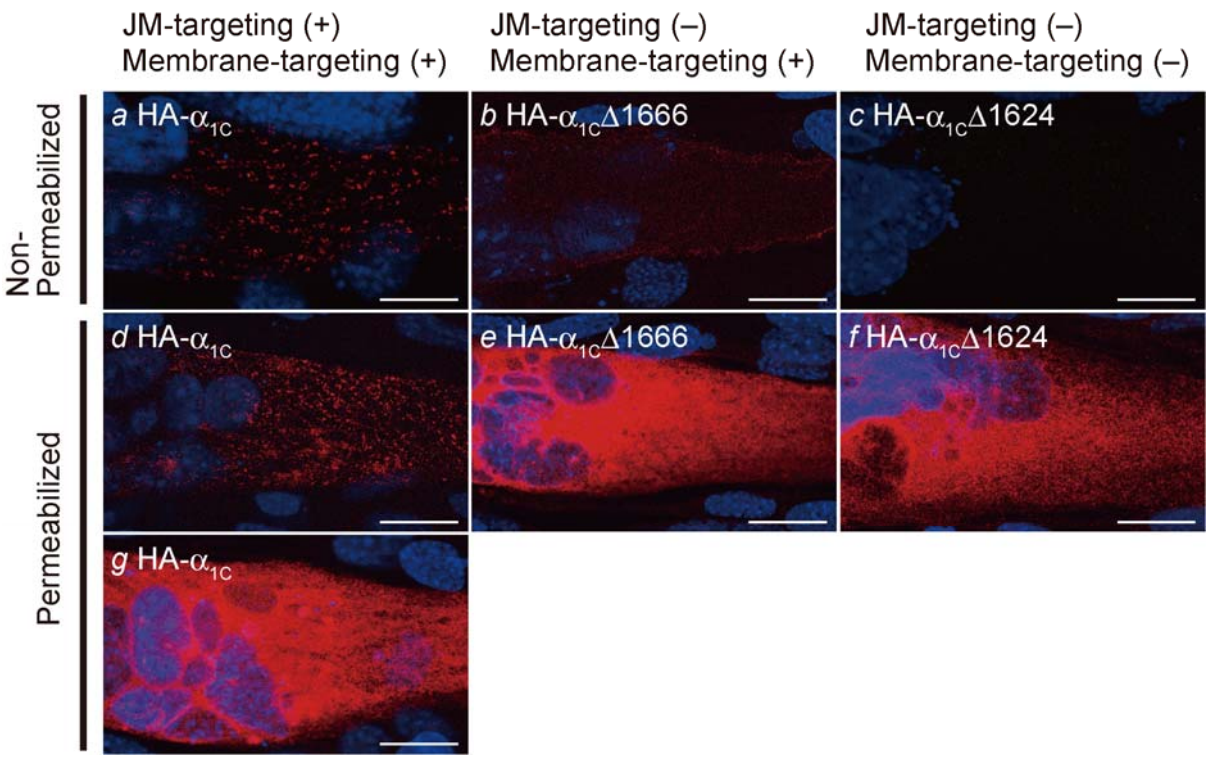
JM-targeting (+)
Membrane-targeting (+)
JM-targeting (–)
Membrane-targeting (+)
JM-targeting (–)
Membrane-targeting (–)
Non-Permeabilized
Permeabilized
a HA-α1C
b HA-α1CΔ1666
c HA-α1CΔ1624
d HA-α1C
e HA-α1CΔ1666
f HA-α1CΔ1624
g HA-α1C

Fig. S2

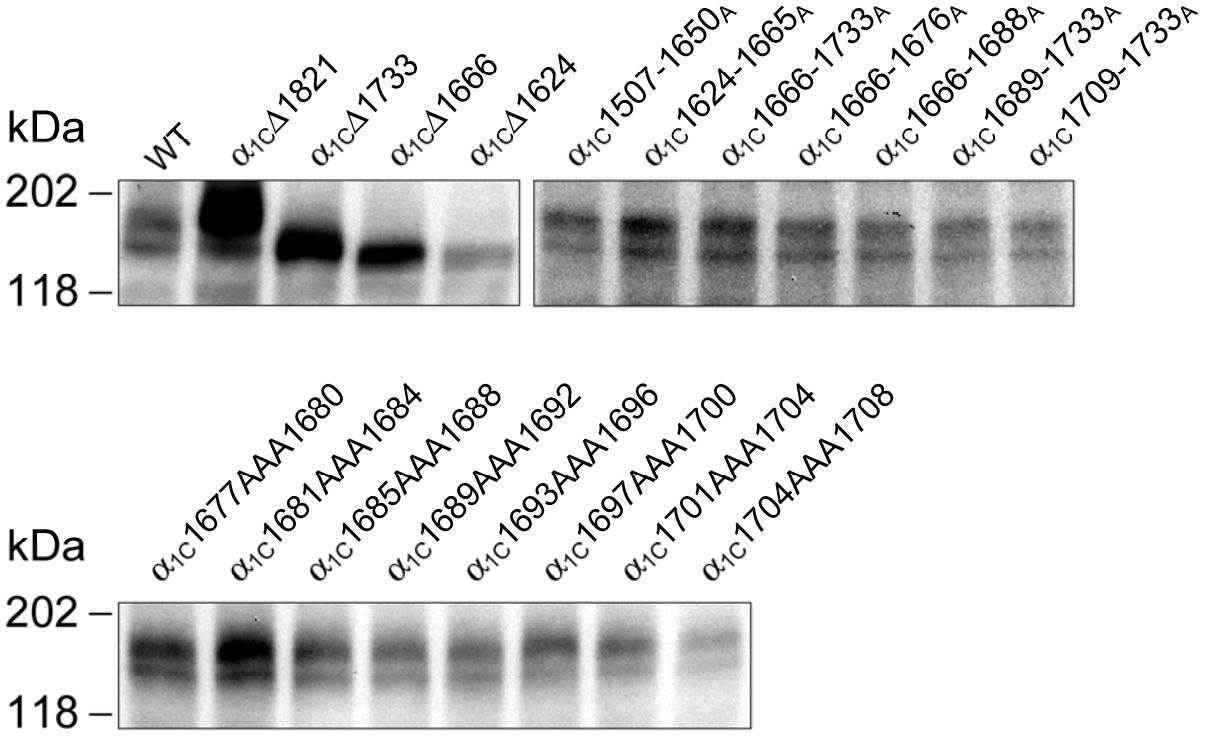
kDa
WT
α1CΔ1821
α1CΔ1733
α1CΔ1666
α1CΔ1624
α1C1507-1650A
α1C1624-1665A
α1C1666-1733A
α1C1666-1676A
α1C1666-1688A
α1C1689-1733A
α1C1709-1733A
202
118
kDa
α1C1677AAA1680
α1C1681AAA1684
α1C1685AAA1688
α1C1689AAA1692
α1C1693AAA1696
α1C1697AAA1700
α1C1701AAA1704
α1C1704AAA1708
202
118

Fig. S3

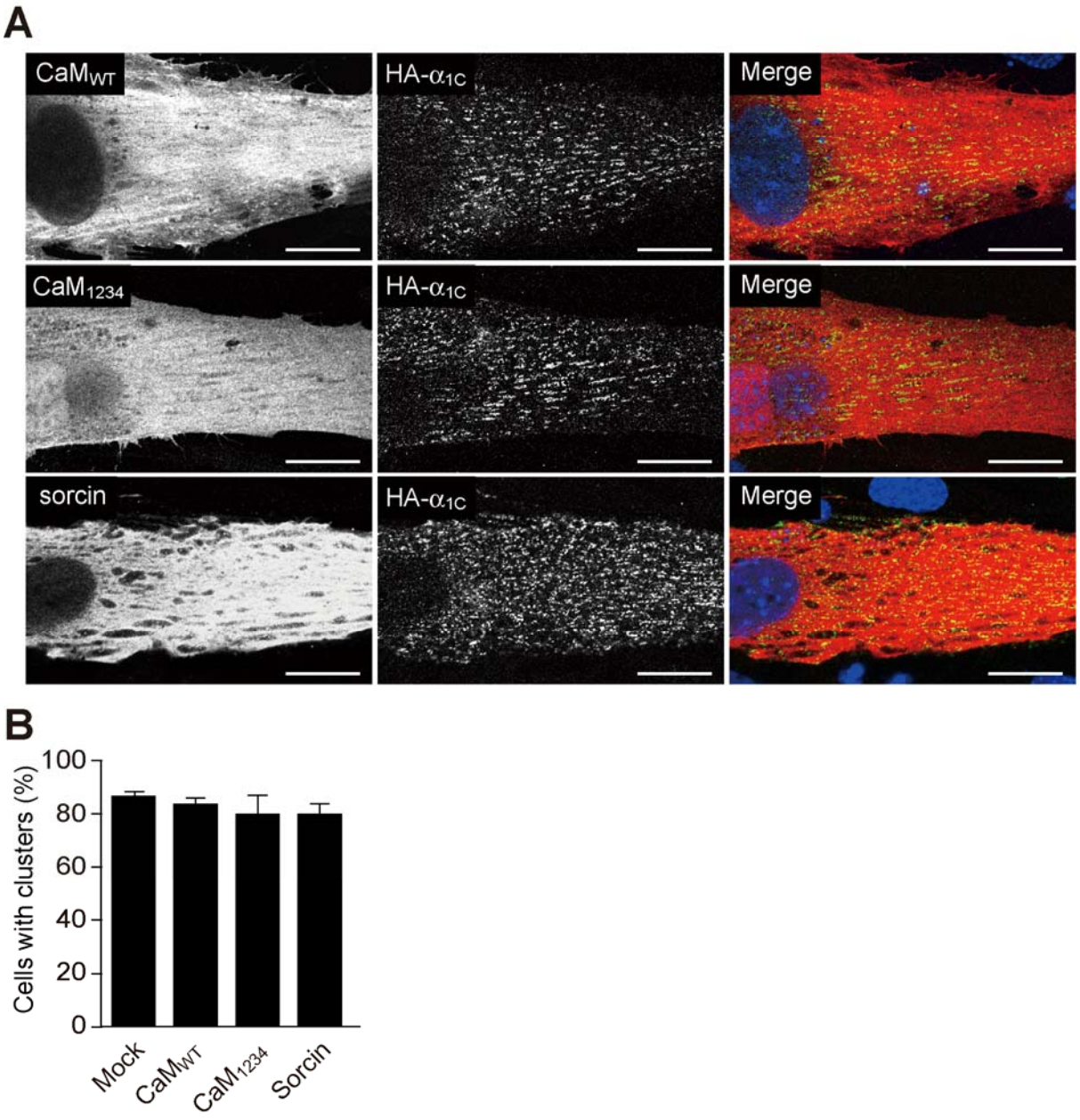
A
CaMWT
HA-α1C
Merge
CaM1234
HA-α1C
Merge
sorcin
HA-α1C
Merge
B
Cells with clusters (%)
100
80
60
40
20
0
Mock
CaMWT
CaM1234
Sorcin

Fig. S4

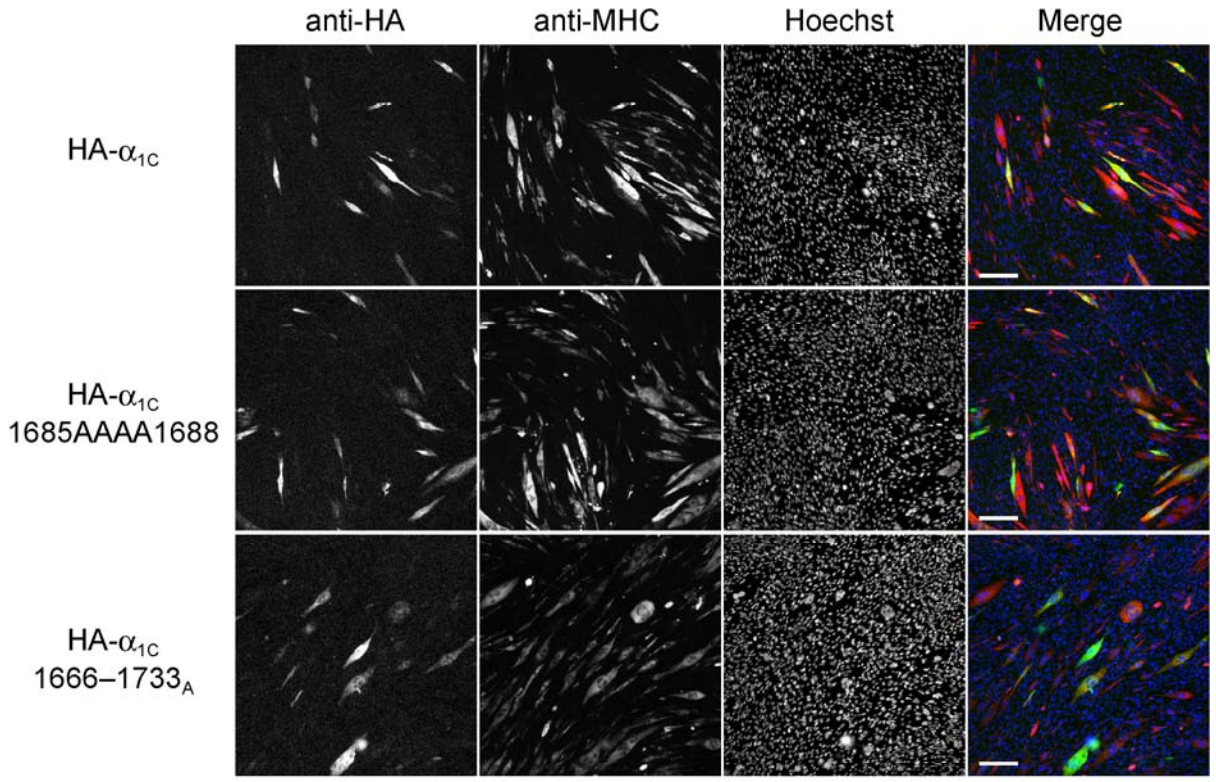
anti-HA
anti-MHC
Hoechst
Merge
HA-α1C
HA-α1C 1685AAAA1688
HA-α1C 1666–1733A

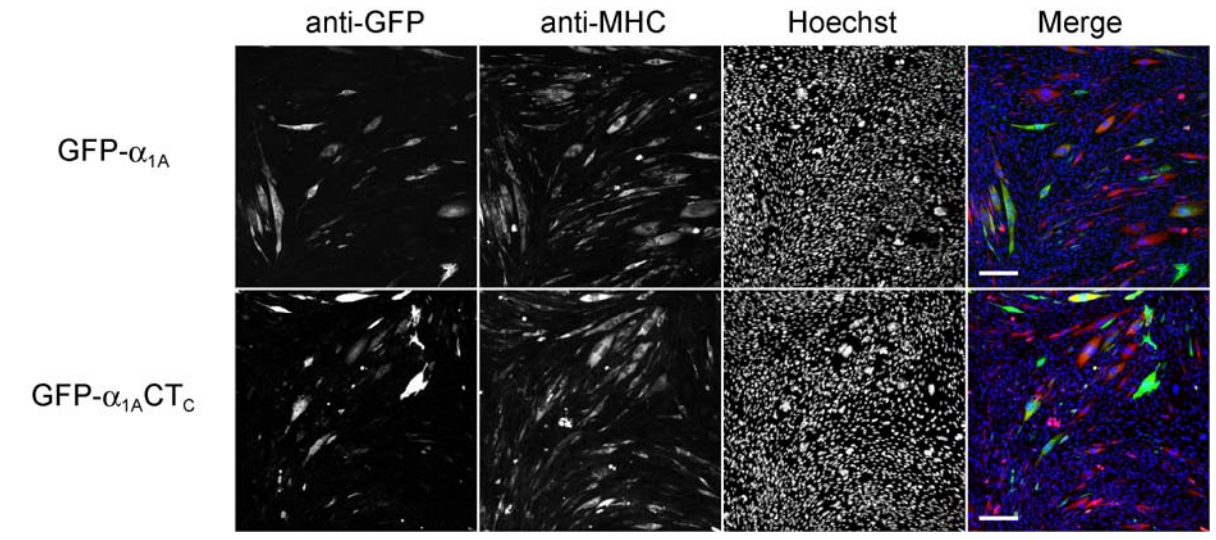
anti-GFP
anti-MHC
Hoechst
Merge
GFP-α1A
GFP-α1ACTC